Palaeogeography, Palaeoclimatology, Palaeoecology 411 (2014) 229–248

Contents lists available at ScienceDirect

Palaeogeography, Palaeoclimatology, Palaeoecology

journal homepage: www.elsevier.com/locate/palaeo

Late Holocene hydrology inferred from lacustrine sediments of Laguna Châltel (southeastern Argentina)

C. Ohlendorf [a,*], M. Fey [a], J. Massaferro [b], T. Haberzettl [c], C. Laprida [d], A. Lücke [e], N. Maidana [d], C. Mayr [f,g,h], M. Oehlerich [g,h], J. Ramón Mercau [d], M. Wille [i], H. Corbella [j], G. St-Onge [k,1], F. Schäbitz [i], B. Zolitschka [a]

[a] GEOPOLAR, Institute of Geography, University of Bremen, Celsiusstr. FVG-M, D-28359 Bremen, Germany
[b] CONICET, CENAC/APN, Fagnano 244, 8400 Bariloche, Argentina
[c] Physical Geography, Institute of Geography, University of Jena, Löbdergraben 32, D-07743 Jena, Germany
[d] Facultad de Ciencias Exactas y Naturales, Universidad de Buenos Aires, Buenos Aires, Argentina
[e] Institute of Bio- and Geosciences, IBG-3: Agrosphere, Research Center Jülich, D-52425 Jülich, Germany
[f] Institute of Geography, University of Erlangen-Nürnberg, Kochstr. 4/4, D-91054 Erlangen, Germany
[g] Department of Earth and Environmental Sciences, University of Munich, Richard-Wagner-Str. 10, D-80333 Munich, Germany
[h] GeoBio-Center, University of Munich, Richard-Wagner-Str. 10, D-80333 Munich, Germany
[i] Seminar für Geographie und ihre Didaktik, University of Cologne, Gronewaldstr. 2, D-50931 Cologne, Germany
[j] Argentine Museum of Natural History, Av. Angel Gallardo 470, Buenos Aires, Argentina
[k] Canada Research Chair in Marine Geology, Institut des sciences de la mer de Rimouski (ISMER), UQAR, Rimouski, Québec G5L 3A1, Canada

ARTICLE INFO

Article history:
Received 9 September 2013
Received in revised form 19 June 2014
Accepted 25 June 2014
Available online 3 July 2014

Keywords:
Lacustrine ooids and pseudomorphs after ikaite
Multiple dating
Bioproxies
XRF-scanning
Lake-level changes
Southern hemisphere westerly winds

ABSTRACT

Hydrological changes that occurred during the last 4700 years have been reconstructed using multi-proxy analyses of sediment cores from the volcanic crater lake of Laguna Châltel (50°S, 71°W). The chronology is based on AMS ^{14}C age modeling constrained by paleomagnetic secular variations. Chemical and physical properties of the lake water together with results of lake-water surface-temperature monitoring, as well as sediment characteristics reveal conspicuous features archived as different sedimentary carbonate phases and morphologies which are attributed to lake-level changes.

Sedimentological, geochemical and biological proxies together suggest the development from an initial playa lake-phase towards a system with progressively rising lake level. In detail, proxies indicate the existence of an ephemeral lake since 4700 cal BP until a glauberite-bearing carbonate crust formed around 4040 cal BP which probably is associated to the globally recognized 4.2 ka event. This crust is interpreted as a desiccation event terminating the ephemeral lake phase. Following this desiccation a shift towards conditions with a positive hydrological balance of Laguna Châltel occurs, which leads to the development of a saline lake with ooid formation between 4040 and 3200 cal BP. Further lake-level increase with initially high minerogenic input until 2700 cal BP resulted in a lake freshening which allowed the preservation of diatoms. Sigmoidal and star shaped carbonate crystals occurred until 1720 cal BP indicating a syn- or post-depositional formation of ikaite. Anoxic conditions and increased deposition of clay and sand through fluvial and eolian input are interpreted as a further lake-level rise and/or a prolonged winter ice cover culminating during the Little Ice Age. The highest lake level was probably reached at that time and since then dropped to its present day height.

Previous studies have shown that the southern hemisphere westerly winds (SWW) exert an oppositional control on hydrological regimes at the eastern and the western sides of the Patagonian Andes. At Laguna Châltel SWW forcing is changing evaporation rates by varying wind intensities, air temperatures and lake ice coverages as well as by precipitation rates (easterly vs. westerly sources of moisture). Our data suggests that the lake-level history of Laguna Châltel reflects changes in the SWW during the last 4.7 ka on the eastern side of the Andes. However, the elevated location of Laguna Châltel on an 800 m high plateau at the leeward side of the Andes potentially leads to a local overprint of the SWW influence on the hydrological balance.

1. Introduction

Terrestrial paleoclimatic information from the southern hemisphere mid-latitudes is scarce due to the prevalence of the Southern Ocean compared to only 2% land. This is especially critical when the global

* Corresponding author.
E-mail address: ohlen@uni-bremen.de (C. Ohlendorf).
[1] GEOTOP Research Center, Montréal, Québec H3C 3P8, Canada.

http://dx.doi.org/10.1016/j.palaeo.2014.06.030
0031-0182/

nature of climatic events should be assessed. Moreover, in southern South America drastic zonal climate differences are caused by the Andes which are perpendicular to the prevailing westerly flow direction of air masses. Thus climate archives are strongly affected by local climate conditions (Fletcher and Moreno, 2011) depending whether the archive is situated on the eastern (Mayr et al., 2007) or the western (Lamy et al., 2010) side of the Andes and at high or low altitude. In this context it is currently debated how the behavior of the southern hemisphere westerly winds (SWW) changed during the Holocene (Kilian and Lamy, 2012). Climate modeling results suggest that a strengthening and a poleward shift of the SWW occurred since the mid-Holocene (Varma et al., 2012). While SWW variations on the western side of the Andes are closely associated to changes in precipitation (Garreaud et al., 2013), the relation of SWW changes to variations in precipitation turns out to be more complex on the eastern side of the Andes (Berman et al., 2012). In order to better characterize the impact of SWW on local climate in southeastern Patagonia, more paleoenvironmental records are needed (Fletcher and Moreno, 2011). In this remote area, the number of high-resolution terrestrial paleoclimatic reconstructions is limited to a few studies (e.g. Markgraf et al., 2003; Gilli et al., 2005b; Zolitschka et al., 2006a; Ariztegui et al., 2007; Haberzettl et al., 2007; Fey et al., 2009; Massaferro et al., 2009; Waldmann et al., 2010; de Porras et al., 2011; Schimpf et al., 2011; Mancini et al., 2013). Paleomagnetic records are also rather scarce in this region (Recasens et al., 2011; Gogorza et al., 2012; Lisé-Pronovost et al., 2013).

We present a paleoenvironmental record from Laguna Cháltel (49°S), a crater lake located on a volcanic plateau east of the Andes in South America. In a multiproxy approach we use biological, sedimentological and geochemical data to investigate the hydrological development of Laguna Cháltel and the paleoenvironmental history of southeastern Patagonia during the last ca. 4700 cal BP. A possible connection of the observed changes with the 4.2 ka event is discussed.

2. Site description

Laguna Cháltel (also known as 'Laguna Azul') is a crater lake located at 49°58′S, 71°07′W at an elevation of 788 masl in the province of Santa Cruz, southern Patagonia, Argentina (Fig. 1a). The lake is situated about 160 km east of the Southern Patagonian Icefield and about 70 km east of the large proglacial lakes Lago Viedma and Lago Argentino (Fig. 1b). Laguna Cháltel (CHA) is located on a volcanic plateau locally known as 'Pampa Alta' (Fig. 1b). It consists of Miocene sediments and Pliocene TiO_2-rich basaltic lavas assigned to the La Siberia and the Laguna Barrosa Basalts (Corbella and Lara, 2008) that are part of the discontinuous N–S-trending belt of Late Pliocene mafic backarc lava formations (D'Orazio et al., 2004).

The region of Laguna Cháltel is characterized by a cool-temperate, semiarid climate with strong winds resulting in steppe and semi-desert vegetation (Paruelo et al., 1998; Zolitschka et al., 2006b). The climate is influenced by the southern hemisphere westerly winds which are strongest during the austral summer between 45°S and 55°S, while during the austral winter they move northward and weaken at 50°S (Garreaud et al., 2009). The Andes produces a major rain shadow effect and forced subsidence over their eastern side creates very dry conditions in Argentinean Patagonia. Due to the remoteness of the research area, local meteorological data are not available. Regional interpolation suggests a mean annual air temperature between 7 °C and 8 °C and a mean annual precipitation around 150 mm (Oliva et al., 2001). However, this data hardly accounts for local topography, especially the high elevation of the 'Pampa Alta' plateau. Satellite images (Fig. 1b) and reports of local people suggest that there is a considerable amount of snow on the 'Pampa Alta' plateau in winter.

The modern vegetation in the wider area around the 'Pampa Alta' plateau is composed of semi-desert, shrub-steppe and grass-steppe. The direct vicinity around Laguna Cháltel is covered by xeric steppe with tussock grasses (*Stipa* spp.) and *Festuca pallescens* as dominant species (Movia et al., 1987). Occurrences of dwarf-shrubs (*Nassauvia*, *Ephedra*, *Azorella*), and thickets of *Verbena* and *Nardophyllum* point to comparatively humid conditions at this high elevation plateau compared to shrub-steppe and semi-desert vegetation at lower elevations.

Steep crater walls rise about 40 m above the present-day lake level. The almost circular lake today has a maximum water depth of 41 m (Fig. 1c). This morphology indicates that Laguna Cháltel probably originated from a maar explosion. Hence the hydrological catchment of the lake is rather small and almost exclusively consists of basaltic rocks. There are several small but presumably permanent inflows entering the lake via three short canyons that are deeply incised into the surrounding volcanic rocks. Fluvial runoff in these canyons is probably strongest and most important during snowmelt at the end of winter, but was also observed in the drier season at the end of the Austral summer (March 2004). At the northern lake shore the largest tributary is incised into ca. 1.0–2.5 m thick subaerial outcrops of silty and sandy lake sediments that are interbedded with layers rich in aquatic moss remains and unsorted, angular rubble probably representing proximal delta deposits. The eastern shore of the lake is built up of large blocks of the volcanic bedrock. Close to the mouth of the northern tributary, drowned dwarf-shrubs below the modern water line of March 2004 indicated a lower lake level shortly before 2004 that permitted the growth of terrestrial plants at this place. In contrast, dead dwarf-shrubs obviously killed by drowning, but occurring in a 1–2 m wide strip above the water line of 2004, indicate a previously higher lake level. Past lake-level changes of higher magnitude are also evidenced by relicts of lake-level terraces along the northern and western shores and by white carbonate crusts that cover the blocky material along the eastern and southern shores. These lake-level terraces and crusts indicate a past lake level high stand ca. 10 m above the lake level of March 2004. Quantitative data about ice cover on the lake in winter are not available. However, the high elevation of the lake, satellite images and reports about ice-coverage of lowland lakes in the area suggest that ice cover on Laguna Cháltel is a common phenomenon (Fig. 1b) and can be expected to persist for a considerable period of time.

3. Material and methods

3.1. Actual limnology

Physico-chemical properties of the water column of Laguna Cháltel were determined along depth profiles and for surface samples. However, due to the lack of year-round data, statements can only be made for the time of sampling in the Austral summer 2004 (2004-03-09). Parameters including water temperature, pH, dissolved oxygen and electric conductivity were measured in the field with a Universal Pocket Meter (Multi 340i, WTW). Likewise, alkalinity was also determined in the field by acidimetric titration against phenolphthalein and a mixed indicator resulting in positive p- und m-values (Alkalinity Test, Merck). In the laboratory, anion and cation concentrations of the same samples were determined using ion chromatography and ICP-MS

Fig. 1. Location and bathymetry. (a) The position of southern Patagonia is highlighted as a black area on the inset globe. Laguna Cháltel (CHA) is located ca. 200 km NNW of the nearest city Río Gallegos (RG). The locations of Laguna Azul (AZU), Laguna Potrok Aike (PTA), Laguna las Vizcachas (VIZ), Lago Cardiel (CAR), Lago Guanaco (GUA) and Laguna Bismark (BIS) are indicated. (b) The higher elevation of Laguna Cháltel on the basaltic meseta 'Pampa Alta' (encircled with a white line) can be deduced from a satellite image taken on 2003-08-23 when the meseta was covered by snow and the lake presumably had an ice cover. (c) The bathymetric map of Laguna Cháltel is superimposed on an aerial photograph on which different gullies are visible. Their positions are indicated in light blue. Positions of the mooring, the water profile and all sediment cores taken in 2004 are shown, with the two cores analyzed in this study highlighted in orange. Area stippled in white indicates the proposed zone of ooid formation.

techniques. Lake water chemistry data were used to calculate supersaturation with respect to calcite (Ohlendorf and Sturm, 2001). Water samples were taken for diatom analyses and conserved with formalin.

In order to obtain high-resolution year-round water temperature data, a mooring string with temperature loggers (Minilog thermistors M-08TR, Vemco Ltd.) was installed at the deepest part of the lake in

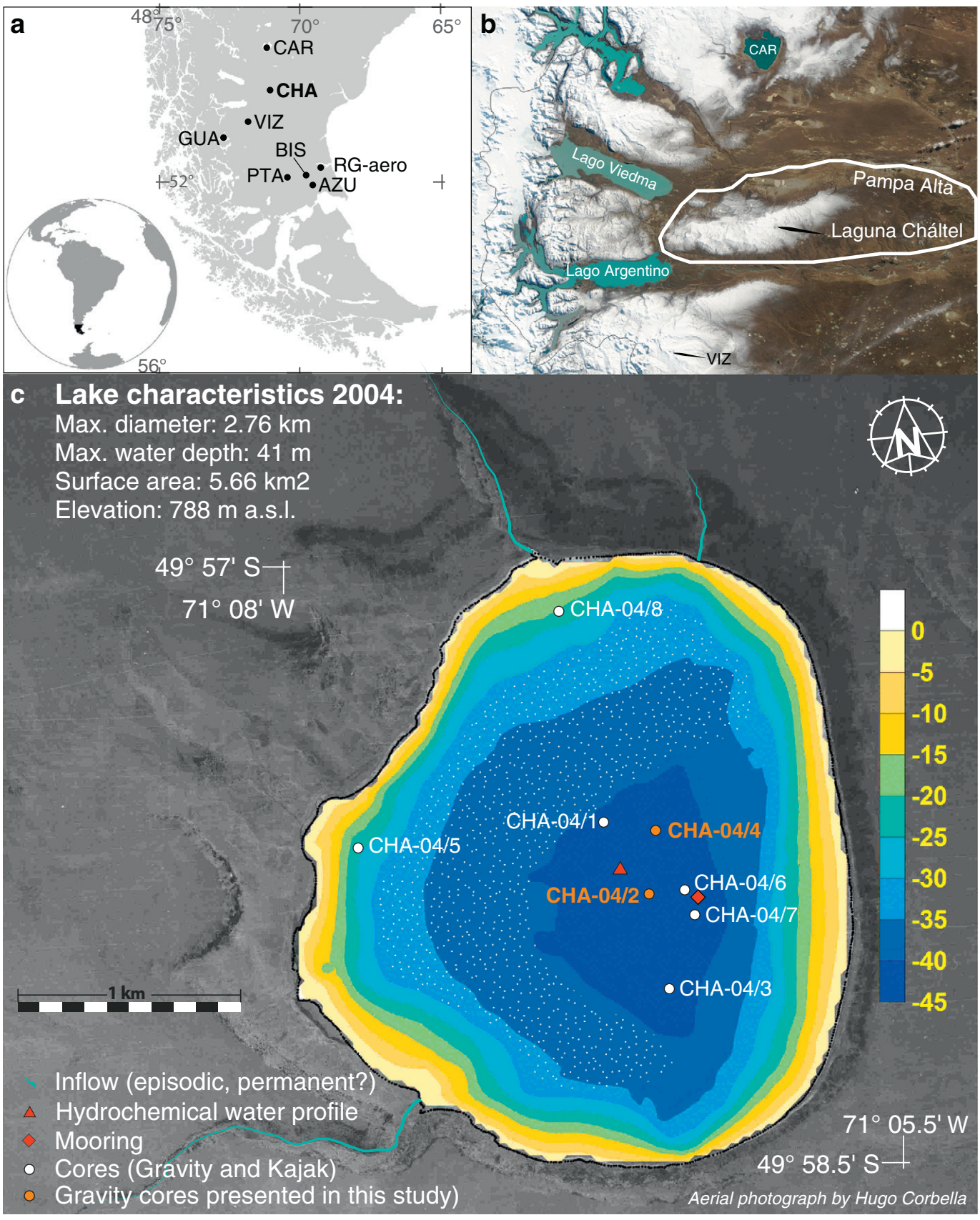

March 2004 (Fig. 1c). Unfortunately, due to a drift of the mooring only surface water temperatures were recorded between 2004-03-10 and 2007-11-14 (dates throughout the paper are expressed according to ISO 8601 as YYYY-MM-DD). For comparison, daily averages of air temperatures were calculated from meteorological data measured at the weather station at Río Gallegos airport (RG-aero, Fig. 1a) available via NOAA/NCDC (NCDC, 2011).

3.2. Coring and sampling

During March 2004, eight gravity cores were recovered from profundal and littoral positions at Laguna Cháltel (Fig. 1c). Sediment cores were sealed gas-tight and stored cool and dark until subsampling. Here we present results of the two parallel cores CHA-04/2 (60.8 cm) and CHA-04/4 (58.0 cm) that were retrieved with a modified ETH-gravity corer (Kelts et al., 1986) from nearby coring positions in the lake center (49°58′S, 71°07′W) at 41 m water depth (Fig. 1c). The cores were split, photographed, described lithologically and smear slides were prepared from selected depths for microscopic investigation. After employing non-destructive magnetic susceptibility and XRF-scanning techniques, cores were volumetrically subsampled in continuous 1 cm intervals (Ohlendorf et al., 2011). Aliquots from each subsample were divided for the different analytical procedures applied. Ostracod, chironomid and diatom were analyzed on core CHA-04/2. For comparison and to test the between-core consistency, core CHA-04/4 was also analyzed for ostracods.

3.3. Chronology

Nine samples were radiocarbon-dated with the accelerator mass spectrometry (AMS) technique at the Poznań Radiocarbon Laboratory, Poland. As no terrestrial macrofossils were available, age determinations were carried out on the fine fraction (<100 μm) of seven bulk sediment samples and on the total inorganic carbon (TIC) fraction of one bulk sediment sample, all from core CHA-04/4. Radiocarbon ages were calibrated with the southern hemisphere calibration curve (SHCal04, McCormac et al., 2004) using the software CALIB 5.0.1 (Stuiver and Reimer, 1993; Stuiver et al., 2005) and are given as calibrated years before present (cal BP). In addition, one sample of a living aquatic moss collected from Laguna Cháltel in March 2004 was dated to test for a potential reservoir effect. The resulting post-modern age was calibrated with the software CALIBomb (Reimer et al., 2004) applying the southern hemisphere data set (Hua and Barbetti, 2004) and is given in calendar years AD.

Age–depth modeling was done using the mixed-effect regression procedure after (Heegaard et al., 2005). The statistical software Tinn-R (Version: 2.3.5.2) and the libraries mgcv and agedepth (Download 24.05.2011: http://www.eecrg.uib.no/Homepages/agedepth_1.0.zip) were applied. Using the one sigma ranges of eight calibrated radiocarbon dates age–depth modeling was done in 1 mm steps between 0 and 58 cm sediment depth of core CHA-04/4 after (Heegaard et al., 2005). After core retrieval in March 2004 the sediment/water interface appeared completely undisturbed in the transparent core liner and the supernatant water was completely clear. Therefore the sediment/water interface was included as an additional date (AD 2004). Ages for depths below the lowermost dated sample taken at 56–57 cm (4440–4520 cal BP) in CHA-04/4 were extrapolated using the average sedimentation rate determined for the nearest two dated samples.

3.4. Paleomagnetic analyses

The natural remanent magnetization (NRM) was acquired at 1 cm intervals on a u-channel from CHA-04/2 using a 2G Enterprises™ 760R cryogenic magnetometer with stepwise alternating field (AF) demagnetization at peak fields of 0 to 100 mT with 5 mT increments. Inclination and declination of the characteristic remanent magnetization (ChRM) were calculated following Mazaud (2005) with AF demagnetization steps from 5 to 75 mT (15 steps). This allows calculation of component magnetizations and Maximum Angular Deviation (MAD) values using principal component analysis (Kirschvink, 1980). ChRM declinations are relative and centered at zero since the core was not azimuthally oriented. Due to the response function of the magnetometer pick-up coils of ~7 cm, the top and bottom ~7 cm of the u-channel have to be considered with caution.

3.5. Physical properties and mineralogy

Water content (WC) and dry density (DD) were calculated from the weights of fresh and freeze-dried volumetric subsamples of core CHA-04/4. Volume specific magnetic susceptibility (κ) was determined on the split cores using Bartington E- and F-sensors employed on an automated measuring bench (Funk et al., 2004). Measurements were performed at 4 mm increments (E-sensor) for CHA-04/2 and at 10 mm increments (F-sensor) for CHA-04/4.

Using the ITRAX core scanner (COX analytical systems, Croudace et al., 2006) X-radiographic images along a 22 mm wide track in the central part of CHA-04/2 were obtained with 200 ms exposure time per 200 μm step interval using a Mo-tube at 50 kV, 30 mA. Gray value analysis was done on the radiograph images with the software ImageJ (ImageJ, 2013).

Grain size measurements were performed continuously at 1 cm intervals for core CHA-04/2 using a Beckman Coulter LS 200 equipped with a variable speed module. Approximately 1 g of fresh sediment was taken directly from the core with a spatula. After removal of macroscopically visible carbonate crystals the sediment was homogenized in an aluminum cup and transferred into centrifuge tubes with 20 ml of a 5% Calgon solution. After 1 min of ultrasonic treatment, samples were transferred to the measuring cell through a 2000 μm sieve and measured at least 5 times for 60 s with sonication turned on during the measurement. When a stable distribution was reached arithmetic means were calculated from at least three individual measurements.

The mineralogical composition of selected samples was determined by standard powder X-ray diffraction (XRD) analyses (Philips X'Pert Pro MD equipped with an X'Celerator Detector Array) using nickel-filtered Cu-Kα(1,2) radiation (λ = 1.541818 Å). Data was collected in the 2 theta-range 2–85° in 0.02° steps with counting times for individual scans of 50 s.

3.6. Geochemistry

Qualitative element counts for major and trace elements were obtained from the split cores using two different X-ray fluorescence (XRF) scanning systems: CHA-04/2 was measured at 1 mm intervals with 10 s exposure time using an ITRAX XRF-core scanner (COX analytical systems, Croudace et al., 2006 at GEOPOLAR, University of Bremen) applying 30 kV/20 mA for the Mo-tube and 30 kV/33 mA for the Cr-tube. Element data and the intensities of the coherent (coh) and incoherent (inc) scatter peaks of Mo and Cr were recorded. CHA-04/4 was measured at 10 mm intervals using a CORTEX core scanner (Jansen et al., 1998) at the ODP/IODP Bremen Core Repository. Values are given as total counts (cts) for CHA-04/2 and as counts per second (cps) for CHA-04/4. XRF-scanning data of core CHA-04/2 are displayed as element ratios with Ti as denominator following Thomson et al. (2006). For the Ti-record coh is used as denominator because it integrates most of the effects that arise from sample matrix variations (Rothwell et al., 2006; Guyard et al., 2007). Concentrations of carbon, nitrogen, sulfur and biogenic silica were determined on core CHA-04/4 at 1 cm intervals. Prior to measurements, freeze-dried subsamples were ground in a mortar and homogenized. Total carbon (TC), total nitrogen (TN) and total sulfur (TS) were analyzed using a CNS elemental analyzer (EuroEA, Eurovector). Concentrations of total organic carbon (TOC) were determined with the same device after successive treatment

with 3% and 20% HCl at 80 °C in order to remove any carbonates. Total inorganic carbon (TIC) was calculated as the difference between TC and TOC. Biogenic silica (BSi) was analyzed with an automated leaching method after Müller and Schneider (1993) and is given as SiO_2. All values are given as weight percentages (wt.%).

3.7. Stable isotopes

Stable isotope ratios of nitrogen ($\delta^{15}N$) and organic carbon ($\delta^{13}C_{org}$) were determined on core CHA-04/4 at 1 cm intervals. Subsamples for isotopic analyses were freeze-dried, homogenized with a spatula and sieved with a 200 μm mesh to eliminate coarse debris of aquatic macrophytes. $\delta^{15}N$ and $\delta^{13}C_{org}$ values were determined on the fine bulk sediment weighed into tin capsules and combusted at 1080 °C in an elemental analyzer (EuroEA, Eurovector) with automated sample supply linked to an isotope ratio mass spectrometer (Isoprime, Micromass). For $\delta^{13}C_{org}$ analysis aliquots were decalcified with HCl (5%) for 6 h in a water bath at 50 °C, afterwards repeatedly rinsed with deionized water to remove the reagent, centrifuged and finally freeze-dried. Isotope ratios are reported as δ values in per mil according to the equation

$$\delta = (R_s/R_{st}-1) \times 1000 \quad (1)$$

with R_s and R_{st} as isotope ratios ($^{13}C/^{12}C$, $^{15}N/^{14}N$) of the samples and international standards VPDB for carbon and AIR for nitrogen, respectively. Analytical uncertainty (one standard deviation based on replicate analyses of samples) was 0.1‰ for $\delta^{15}N$ and $\delta^{13}C_{org}$.

3.8. Biological proxies

Ostracods were prepared according to standard procedures (Holmes, 2001). Individuals were identified according to Martens and Behen (1994), Rosetti and Martens (1998), Meisch (2000), Schwalb et al. (2002), and Cusminsky et al. (2005).

For chironomid analysis, samples were prepared according to the methodology of Walker (1990). Head capsules (HC) were identified with reference to available taxonomic literature (Cranston, 2000; Massaferro and Brooks, 2002) and the Patagonian subfossil chironomid taxonomic identification guide (Massaferro et al., 2013b).

For diatom analysis, sample treatment and slide preparation were carried out following standard procedures (Battarbee, 1986).

Flux values for ostracods, chironomids and diatoms were calculated as the number of individuals considering the sedimentation rate.

3.9. Statistical analysis

Bioproxy zones were established by optimal partition (Birks and Gordon, 1985) and significance of the partitions was assessed by the Broken-stick model (Bennett, 1996).

Zonation was performed considering species accounting for at least 3% of their corresponding assemblage in at least one sample. Relative abundances were recalculated to add up to 100% between all species at each level and were defined by optimal partitioning.

4. Results

4.1. Actual limnology

The course of the surface water temperatures of Laguna Cháltel closely follows that of air temperatures determined at RG-aero (Fig. 2a, b). Surface water temperature shows a clear seasonal signal with a temperature below 1 °C between June/July and September/October and above 8 °C between January and April/May (Fig. 2b). During the observation period, the annual maximum surface water temperature decreased from 13 °C in 2005 to 10 °C in 2007 and the date when this temperature was reached moved from 19th of February in 2005 to 25th of January in 2007. No major time lags were registered between air and water temperatures.

In the Austral summer 2004 (2004-03-09), Laguna Cháltel exhibited a slight stratification of the water body with temperatures in the epilimnion (0–2 m water depth) of 12.2 °C near the surface and 10.6 °C in the hypolimnion below 5 m water depth (Fig. 2c). Water column pH values ranged from 9.0 in the epilimnion to 8.8 in the hypolimnion. Oxygen concentrations were between 9.7 mg l^{-1} in the epilimnion and 7.8 mg l^{-1} in the hypolimnion. Electric conductivity did not display any stratification and showed values around 788 μS cm^{-1} throughout the entire profile. Alkalinity of the surface water was 8.7 mmol l^{-1} (pos. m-value) and 1.1 mmol l^{-1} (pos. p-value).

Mean nutrient concentrations at the sampling date (2004-03-09) were 0.14 mg l^{-1} for nitrate, 0.388 mg l^{-1} for total phosphorus and 2.28 mg l^{-1} for silicon with the latter showing considerable variation within the water column (Fig. 2c). Super-saturation with respect to calcite varied between 10 and 40 times (Fig. 2c). Water chemistry was characterized by a dominance of the carbonate ion (mostly HCO_3^- at the given pH) and high Na^+ concentrations (Fig. 2d).

4.2. Lithology

All cores taken from the central basin of Laguna Cháltel, i.e. CHA-04/1, 2, 3, 4, 6 and 7 show a very similar lithologic succession and can be correlated by means of characteristic lithologic features. This is exemplified for cores CHA-04/2 and CHA-04/4 in Fig. 3. Because CHA-04/2 is the longest core, its lithostratigraphy is described below from the top to the base of the core. The lithologic units defined in this core are also encountered in the other cores in slightly different sediment depths. The mineralogical composition was determined for selected representative samples from each lithologic unit. The main minerals occurring are listed in Fig. 3 in descending order of their estimated content.

Unit A (0 to 9.5 cm sediment depth) is composed of grayish-brown, layered, sandy silt. The uppermost 1 cm shows a reddish brown color. At 2.5 cm, a layer with frequent bivalve shells occurs. Between 4 and 6.5 cm, brownish gray to black lamination is observed, best visible in CHA-04/4 at 5-8 cm (Fig. 3) because this photograph was taken directly after core opening and before oxidation could commence. Occasionally, up to 3 mm long, sigmoidal carbonate crystals occur between 7.5 and 9.5 cm. The main minerals that occur in this unit are quartz (Qz), feldspars (Fsp), calcite (Cc) and phyllosilicates (Phy).

Unit B (9.5 to 26.0 cm) consists of grayish light brown, layered silt. Up to 3 mm large, sigmoidal or star shaped (Fig. 3), yellowish light brown, carbonate crystals are scattered throughout this unit. At the base of this unit a layer with reddish dark brown spots occurs in CHA-04/2 which is not obvious in CHA-04/4. Black mackles as well as black sand grains are scattered throughout this unit as well. A layer with brownish gray to black lamination occurs at 18.5 to 19.5 cm in CHA-04/4 but is not obvious at the corresponding level (15.5 to 16.5 cm) in CHA-04/2. Qz is followed by Cc, Fsp and Phy in the mineralogical composition.

Unit C (26.0 cm to 51.5 cm) is characterized by brownish gray, layered sandy silt. Several reddish brown layers occur in this unit and a layer with brownish gray to black lamination is observed around 42.5 cm. The mineralogical composition is dominated by Qz, followed by Fsp, Cc and Phy. At the base of this unit a blackish to dark brown silty sand layer with irregular base and top boundaries occurs between 50.0 and 51.5 cm. This layer consists of rounded dark colored rock fragments that in some cases are coated by a thin, light colored, porous crust. A distinctive whitish, light gray, carbonaceous layer is observed at 48.5 cm. A characteristic feature of this unit is the scattered occurrence of well-rounded carbonate ooids of up to 200 μm in diameter (Fig. 3). Layers in which ooids are enriched occur at 26 and at 36 cm.

Unit D (51.5 cm to 60.8 cm) reveals yellowish and reddish dark brown to light brown, layered sandy silt. Qz is the dominant mineral followed by Cc, Fsp and Phy. A distinctive whitish, light gray,

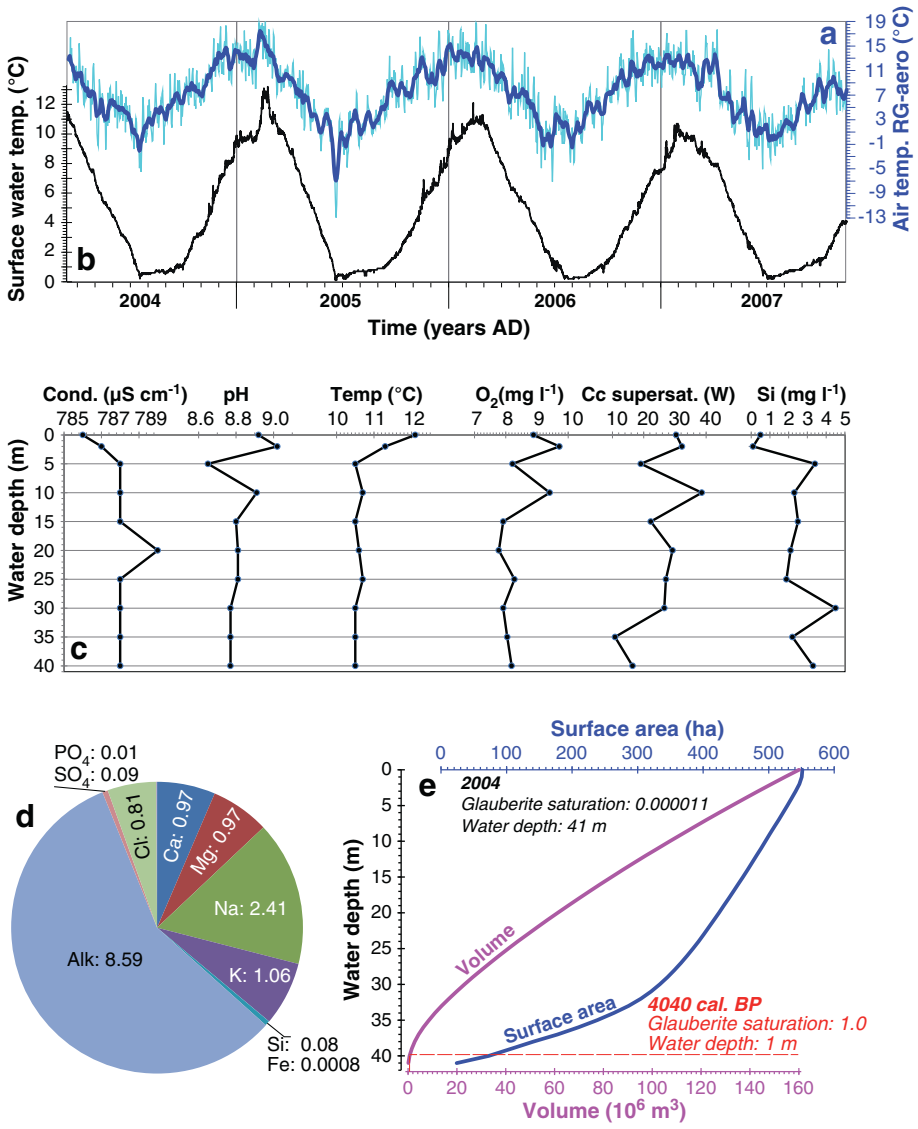

Fig. 2. Water chemistry profile and surface temperature series. (a) Daily averages of air temperature (thin blue line) recorded at the meteorological station Río Gallegos airport (RG-aero in Fig. 1a). Thick blue line represents the 9 point running mean. (b) Surface water temperatures recorded by a temperature logger at Laguna Cháltel between 2004-03-10 and 2007-11-14. (c) Depth profiles of conductivity, pH, temperature, oxygen concentration, super-saturation with respect to calcite and silicon concentrations from 0 to 40 m water depth as determined on 2004-03-09. (d) Pie chart visualizing the ion composition (given in mmol l^{-1}) of the lake surface water at the same date. (e) Hypsographic curve of Laguna Cháltel together with values for the water-depth at today's glauberite saturation and at the point when glauberite precipitation would start (see text for explanation).

carbonaceous layer occurs between 54.5 and 55.5 cm as well as at the base of the core below 59.5 cm. The most striking feature of this unit is a light brownish yellow, carbonaceous, sandy silt layer between 51.5 and 52.0 cm. This layer has an irregular surface and consists of very hard sediment chips (Fig. 3) composed of sand grains of different colors that are cemented by a carbonaceous matrix. XRD analysis of this layer reveals Cc as the main component followed by Qz, Fsp and Phy. As a minor component, glauberite ($Na_2Ca(SO_4)_2$) was detected.

4.3. Core correlation

The cores CHA-04/2 and CHA-04/4 were correlated by wiggle-matching of macroscopically visible marker layers (e.g., the carbonate layer at 51 cm in CHA-04/4), their ostracod assemblages and Ti peaks determined by XRF-scanning (Fig. 3). Between tie points, sediment depths were calculated by linear interpolation. A common depth scale was calculated at 1 cm intervals by projecting the depth scale of CHA-04/2 onto the depth scale of CHA-04/4. Using this correlation the chronology established for CHA-04/4 was transferred to CHA-04/2. In order to check the robustness of this correlation, the magnetic susceptibility record for both cores was plotted on the common depth scale of CHA-04/2 and shows good visual agreement (Fig. 3).

4.4. Chronology

The radiocarbon dates from the sediment sequence of core CHA-04/4 exhibit ages between 190 ± 30 and 4080 ± 30 ^{14}C yrs BP. Calibrated ages range between 0 and 4520 cal BP (Table 1). The sample of living aquatic moss reveals a post-modern value (113.2 ± 0.3 pMC) and post-bomb calibration results in two intersections with the calibration curve and thus two possible ages: AD 1959 or AD 1993 (Table 1). A basal age of 4620 cal BP is obtained for CHA-04/4. The resulting age model shows a sigmoidal shape (Fig. 4). Accordingly, the sedimentation rates (SR) calculated every 1 mm for core CHA-04/4 by division with the

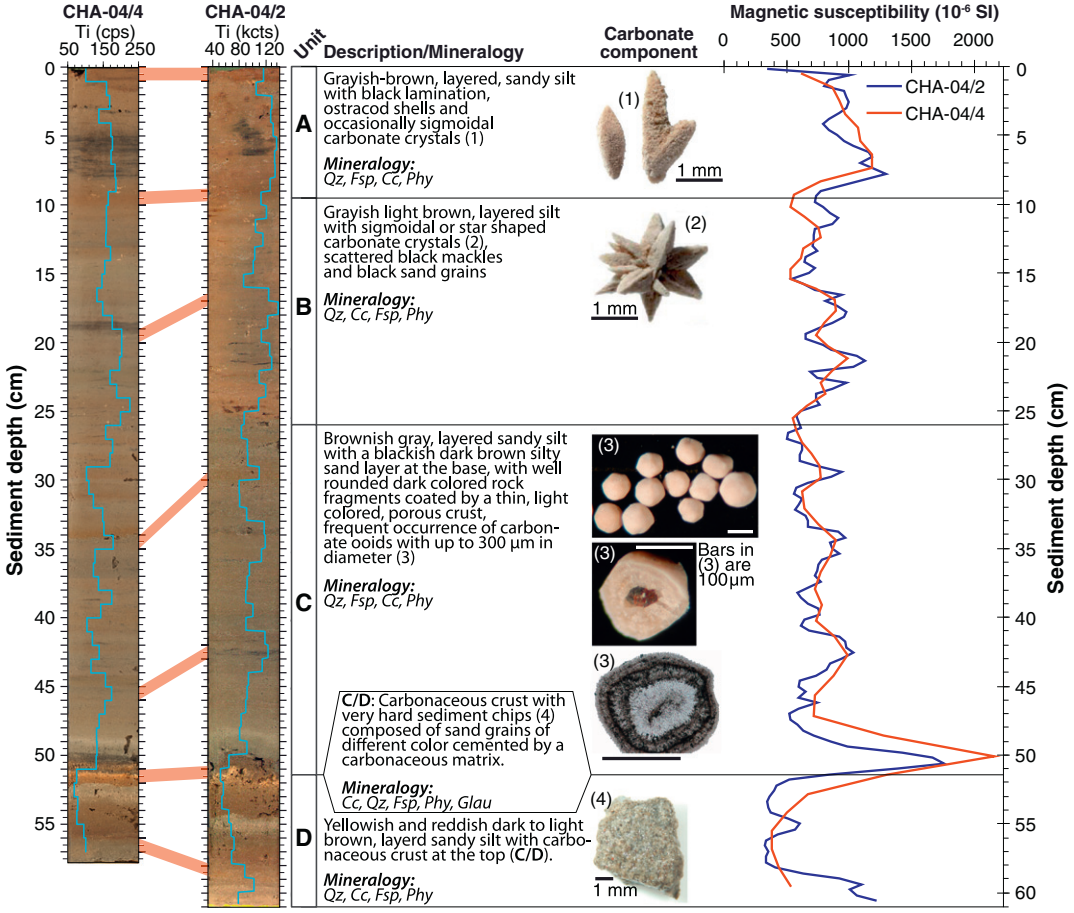

Fig. 3. Correlation of cores CHA-04/2 and CHA-04/4. Correlation levels are indicated by light red bars. The Ti-records (blue curves) were used to aid correlation of cores. A short description and the mineralogical composition of the four distinguished lithologic units are given. Minerals are listed in descending order of their quantities in the samples (Qz = quartz, Cc = calcite, Fsp = feldspars, Phy = phyllosilicates, Glau = glauberite). For each unit photographs of characteristic carbonate components are shown. Magnetic susceptibility is shown for both cores projected on the depth scale of CHA-04/2.

respective modeled age are very low (<0.1 mm yr^{-1}) in the topmost 15 cm of the core (Fig. 4). Below this depth a maximum of 0.54 mm yr^{-1} is reached at 31 cm sediment depth. SR then decrease again to values around 0.11 mm yr^{-1} at the base of the core.

The age model shows a relatively narrow 95% confidence interval (Fig. 4). The maximum difference between the lower and the upper level of the confidence interval is 418 years. The chronology obtained for CHA-04/4 was then transferred to CHA-04/2 using the correlation outlined above (Fig. 3). Since the latter core is slightly longer an extrapolated basal age of 4660 cal BP was obtained for it.

4.5. Paleomagnetic secular variations

Except for the upper part of the record which is affected by an edge-effect, MAD-values are always lower than 5° (Fig. 5). NRM intensities are high and range between 6.8×10^{-2} and 1.3×10^{-3} A m^{-1} (Fig. 5). Inclination ranges between 66.9°S and 41.3°S, the latter value being affected by the edge effect at the top of the u-channel (Fig. 5). The expected geocentric axial dipole (GAD, 67.21°S for Laguna Cháltel) is only observed at the top of the record. In the remaining part the inclination is shallower than the expected GAD value (Fig. 5). Resulting from the low temporal resolution in the upper part of the record, graphs for inclination and declination are very smooth when plotted on an age scale (Fig. 5). In order to see the temporal data coverage, each data point is shown for Laguna Cháltel in Fig. 5. In contrast, for the lower part of the record where sedimentation rates are higher, clear variations in declination and inclination are observed.

4.6. Physical properties

The highest dry density values (up to 0.67 g cm^{-3}) were detected at 49–51 cm. Apart from this local maximum dry density varies around the mean value of 0.25 g cm^{-3} in the lowermost part of the core between 59 and 13 cm (Fig. 6). A gradual upwards increase of dry density from the mean to values as high as 0.54 g cm^{-3} occurs between 13 cm and 1 cm whereas in the uppermost 1 cm of sediment dry density decreases again to 0.26 g cm^{-3}.

Variations in gray values from the sediment X-radiographs (Fig. 6) reflect changes in sediment wet bulk density with low values, i.e. darker sections on the image, being indicative of a higher density. The most striking features are local density maxima below 50 cm and a density increase towards the top in the uppermost 11 cm.

Magnetic susceptibility (Fig. 6) exhibits moderate variations around a mean value of 770×10^{-6} SI for most of the profile. However a prominent peak with values up to 1770×10^{-6} SI is observed at 49–52 cm.

Ooids do not occur in units A and D but were only detected in lithologic units B and C of CHA-04/2 (Fig. 6). Ooids are enriched in the medium sand fraction (200–630 µm) and exhibit two distinct maxima. A lower peak with up to 1652 ooids cm^{-3} is centered at 42.5 cm and contains ooids with a dull surface. An upper, broad peak with up to 1639 ooids cm^{-3} is centered at 33.5 cm and contains ooids with a polished surface. From this upper peak the ooid abundance decreases gradually from 33.5 cm until values around 0 are reached at 17.0 cm.

Table 1
AMS ^{14}C ages of Laguna Cháltel sediment core CHA-04/4 and modern sample PAIS 175. Columns labeled with 'model age' denote the top and bottom ages of each sample that results from the age modeling after Heegaard et al. (2005). pMC = percent modern carbon.

Sample core	Depth top (cm)	Depth bot. (cm)	Depth mean (cm)	Material	Lab no. Poz-	Age ^{14}C (yrs BP)	Error ^{14}C Age (y)	Median age (cal BP)	Min 2σ age (cal BP)	Max 2σ age (cal BP)	Model mean (cal BP)	Model top (cal BP)	Model bot. (cal BP)
PAIS 175	Water/ modern	Water/ modern	Water/ modern	Submersed aquatic moss, sampled as living plant in Lag. Cháltel in March 2004	8490	113.2 pMC	+/− 0.3 pMC	AD 1959 or AD 1993	AD 1996	AD 1959	−59	−75	−44
CHA 04/4	0.5	1.4	0.95	Fine fraction (<100 μm) of bulk sediment	10554	190	+/− 30	177	0	286	50	−212	311
CHA 04/4	3.5	4.5	4.00	Fine fraction (<100 μm) of bulk sediment	11608	455	+/− 30	485	335	518	512	437	587
CHA 04/4	7.0	8.0	7.50	Fine fraction (<100 μm) of bulk sediment	11609	1410	+/− 30	1286	1183	1332	1275	1206	1344
CHA 04/4	12.0	13.0	12.50	Fine fraction (<100 μm) of bulk sediment	10555	2260	+/− 30	2233	2133	2329	2216	2024	2408
CHA 04/4	18.5	19.5	19.00	Fine fraction (<100 μm) of bulk sediment	8475	2790	+/− 35	2827	2756	2924	2823	2701	2946
CHA 04/4	33.0	34.0	33.50	Fine fraction (<100 μm) of bulk sediment	8450	3090	+/− 35	3251	3081	3359	3252	3042	3461
CHA 04/4	51.1	51.3	51.20	TIC dated	8503	3740	+/− 35	4024	3898	4147	4022	3825	4219
CHA 04/4	56.0	57.0	56.50	Fine fraction (<100 μm) of bulk sediment	10556	4075	+/− 30	4485	4415	4780	4477	4349	4606

The grain size of CHA-04/2 cannot strictly be used for inferring clastic input into Laguna Cháltel, because carbonates were not destroyed but large carbonate crystals were removed prior to grain size analysis. Hence the occurrence of sand sized carbonate ooids in some sections is reflected in the sediment grain size distribution. Regarding the complete record (Fig. 6) the average composition of the CHA-04/2 sediments is 13.3% sand, 81.2% silt and 5.6% clay. Most pronounced variations are observed in the coarse silt to fine sand fractions and in the clay fraction. The latter ranges below 3% between 21 and 61 cm but is always above 6% in the topmost 21 cm of the core. The most striking variations occur in the fine sand fraction (63–250 μm). At the bottom of the core, below 50 cm, fine sand percentages exhibit highest values of up to 42% occurring at 51–52 cm. Slightly smaller peaks occur at 54–56 cm and 58–59 cm. In these layers, significant amounts of medium and coarse sand were also detected. From 50 to 21 cm, fine sand percentages gradually decrease from about 20% to 0% with the coarsest particles occurring between 40 and 50 cm. Between 21 and 11 cm fine sand practically disappears (0 to 1%) but constitutes up to 18% again in the topmost 11 cm of the core.

4.7. Bulk organic geochemistry

The TS concentration curve (Fig. 7) is characterized by two broad peaks at 5–12 cm and 18–24 cm. In all other intervals, TS concentrations are below the detection limit.

BSi concentrations (Fig. 7) increase gradually from the bottom (0.8 wt.% at 50 cm) to the top of the core (12.4% at the sediment surface). BSi values depict small fluctuations below 23 cm, whereas above larger fluctuations superimposed on a gradual increase occur. A weak linear correlation between BSi and TOC exists ($r = 0.54$).

TOC (Fig. 7) and TN (not shown) concentrations depict mean values of 2.8 wt.% and 0.27 wt.%, respectively and are strongly correlated ($r = 0.89$). Minimum values as low as 1.1 wt.% and 0.1 wt.% were detected at the transition from unit C to D and at the base of the core (61 cm). Maximum values of up to 4.9 wt.% and 0.54 wt.%, respectively, occur at the transition of unit A to unit B and at the top and near the base of the core.

TIC values (Fig. 7) show a general trend towards decreasing values from the bottom to the top of the core. However, rather large fluctuations are observed, with the highest concentrations of up to 4.4 wt.% occurring at 51–53 cm and the lowest (0.2 wt.%) at the sediment surface.

The TOC/TN molar ratio (Fig. 7) varies around a mean value of 11.5 between 23 and 61 cm. A transition to lower values occurs between 20 and 23 cm. Between 0 and 20 cm variations around a mean of 9.1 are observed.

Stable isotope values of organic carbon ($\delta^{13}C_{org}$) vary only slightly around −25.5‰ below 51.5 cm. $\delta^{13}C_{org}$ values show a local maximum of −22.9‰ at 51.5 cm and an abrupt decrease to −27.0‰ at 49 cm. Between 49 and 14 cm, $\delta^{13}C_{org}$-values slightly increase to −27.8‰. Above 14 cm $\delta^{13}C_{org}$ values increase to the maximum value of −21.7‰ in the topmost 1 cm of the core (Fig. 7).

Stable isotope values of nitrogen ($\delta^{15}N$) range between 5.5 and 7.5‰ below 16 cm except for the interval between 43 and 49 cm where maximum values of 10.5‰ are reached. Above 16 cm $\delta^{15}N$-values decrease gradually from 7.8‰ to 3.7‰ in the uppermost 1 cm of the core (Fig. 7).

4.8. Bulk inorganic geochemistry

The inorganic geochemistry data determined by XRF-scanning is shown in Fig. 8 and is always displayed as deviation from the average value with positive/negative deviations shown as colored shading in Fig. 8. Whereas element/Ti ratios (Fig. 8) are considered to reflect variations in the mineralogical composition of the detrital matter itself, the Ti/coh ratio (Fig. 8) is considered to reflect variations in the overall input of detrital minerogenic matter.

The S/Ti-ratio mirrors the TS curve with peaks at 8–10 and 19–22 cm (yellow). An additional peak is observed at 4.5 cm. Peaks are sharper

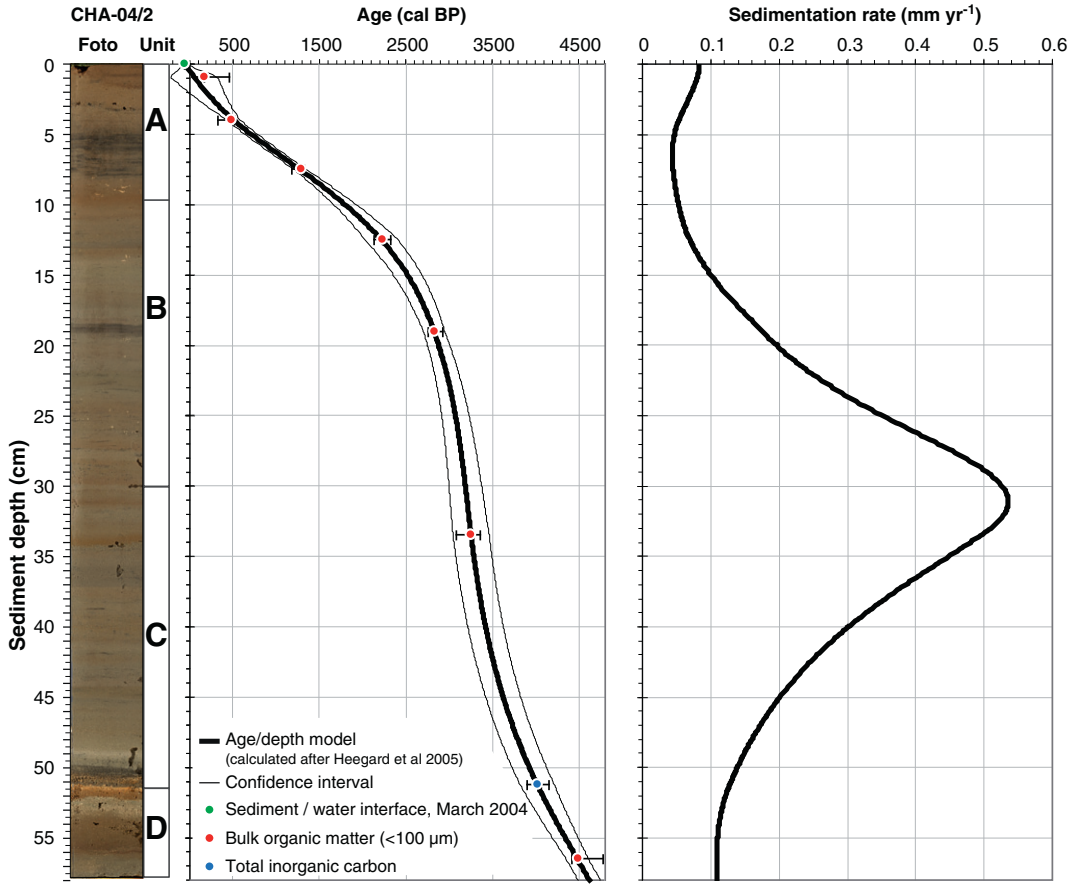

Fig. 4. Age model as determined by the mixed effect regression procedure (Heegaard et al., 2005) of 8 samples taken from core CHA-4/4 for AMS ^{14}C dating. Sedimentation rates are shown on the right panel. Transfer of the chronology to core CHA-04/2 was achieved using the correlation shown in Fig. 3.

owing to the higher resolution of the XRF-measurements (1 mm) compared to the conventional TS analyses (10 mm).

The Fe/Ti-ratio fluctuates around its mean of 35 with no detectable long-term trend. Peaks above/below average are shown in yellow/green.

The Mn/Ti-ratio shows high amplitude variations (note logarithmic scale in Fig. 8) around the mean of 0.62 with peaks of high intensities (green) e.g. in the uppermost 1.0 cm of the core. A pronounced minimum (yellow) occurs between 4.0 and 8.0 cm.

The 11-points running correlation between Fe and Ti is always positive with $r > 0.5$ (green) below 26 cm, but peaks with an inverse correlation of $r < -0.5$ (yellow) occur above 26 cm.

The Ca/Ti-ratio shows high amplitude fluctuations and is therefore displayed on a logarithmic scale in Fig. 8. Distinct peaks above (magenta) the mean of 2.8 occur at 1, 11, 37 cm and below 49 cm, while for most parts of the record Ca/Ti ranges below (gray) the mean value.

The Zr/Ti-ratio (displayed as 7-point running mean in Fig. 8) exhibits peaks above average (blue) around 48, 51 and 55 cm and a gradual increase in unit A. Values below average (red) occur between 34 and 47 cm (unit C) and in most of unit B.

The coh/inc-ratio exhibits narrow peaks above average (blue) in units A to C and wider peaks in unit D whereby a gradual increase occurs from 12 cm towards the top of the core.

The Si/Ti-ratio in unit D exhibits two peaks centered at 51.5 and 55 cm (blue). In unit C, the Si/Ti-ratio is at a constantly low level (red) and increases only at the transition to unit D. From the boundary between units B and C at 26 cm the Si/Ti-ratio increases linearly towards the top of the core (blue).

The K/Ti-ratio exhibit values above average (blue) in units A and D and mostly below average (red) in units B and C.

The Ti/coh-ratio exhibits an overall increasing trend from the bottom to the top of the core. Lowest values (red) occur at 50–59 cm in unit D. Peaks with highest values (blue) occur in the lower half of unit B, whereas values are almost constantly above average in unit A.

4.9. Bioproxies

Optimal partitioning based on all bioproxies allowed the delimitation of four statistically significant bioproxy assemblage zones (BAZ) in the stratigraphical sequence (Fig. 9).

BAZ-D (4655–3920 cal BP) is characterized by the dominance of *Limnocythere rionegroensis* (up to 95% of the ostracod assemblage). Other species present, which account for almost 30% of the ostracod assemblage in some samples, are *Limnocythere patagonica*, *Eucypris virgata*, *Eucypris fontana* and *Eucypris cecryphalium*. The only chironomid taxa present in this zone is *Polypedilum*. Diatoms are absent.

In BAZ-C (3920–3185 cal BP), diversity of all bioproxies is the lowest of the whole sequence. Apart from a couple of isolated peaks of the chironomid *Polypedilum*, there is a complete absence of chironomid and diatom remains. The ostracod *Limnocythere rionegroensis* is the dominant species (between 90 and 100%). Towards the top of the zone, diatoms appear marking the onset of BAZ-B.

In BAZ-B (3185–1630 cal BP), the diatom assemblage is dominated by *Thalassiosira patagonica*, *Cocconeis placentula* var. *euglypta* and *Epithemia adnata*. Around 2400 cal BP, *Hyalodiscus* sp. appears and dominates the assemblages (ca 80%) until the top of the zone when it starts to decrease. At the base of the zone, the ostracod *Limnocythere patagonica* reappears and *Limnocythere rionegroensis* decreases to its final disappearance towards the top of this zone. There are also some abundance spells of *Kapcypridopsis megapodus*. Although

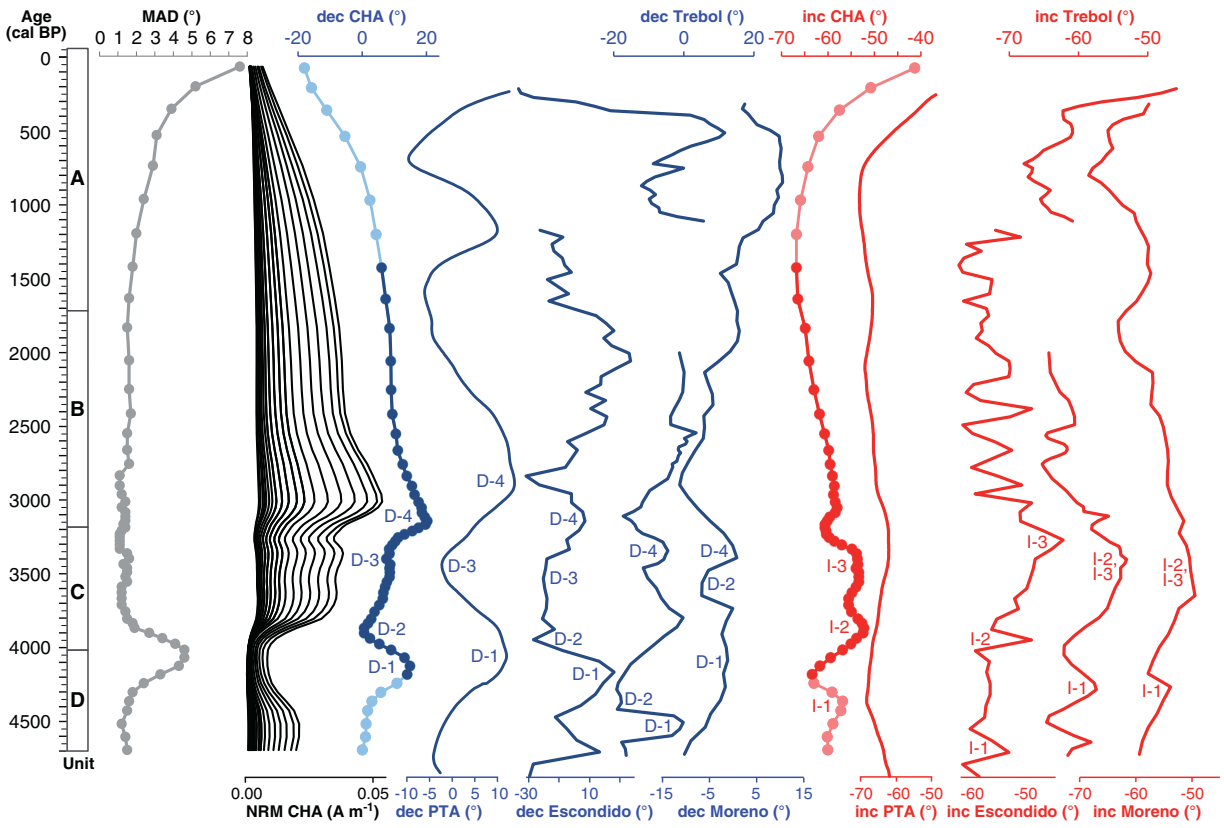

Fig. 5. Paleomagnetic data determined on the Laguna Cháltel core CHA-04/2 shown against age (cal BP), lithologic units are displayed on the left side. Maximum Angular Deviation (MAD), as well as downcore variations of the NRM at all demagnetization steps (each black line represents 5 mT increments from 0 to 80 mT and 10 mT increments from 80 to 100 mT) are shown on the left panels. Declination (blue) and inclination (red) records from Laguna Cháltel are compared with records from lakes Potrok Aike, PTA (Lisé-Pronovost et al., 2013), Escondido (Gogorza et al., 2002), Trébol (Irurzún et al., 2006) and Moreno (Gogorza et al., 2000).

in low abundances, two chironomid taxa appear for the first time: *Cricotopus* and *Phaenopsectra*.

BAZ-A (1630 cal BP up to the present) is characterized by a compositional change of all bioproxies. *Cyclostephanos salsae* appears as dominant diatom species. *Hyalodiscus* sp. disappears and *Cocconeis placentula* var. *euglypta* and *Epithemia adnata* show their minimum values. Among the ostracods, a complete replacement of *Limnocythere rionegroensis* by *Limnocythere patagonica* and *Kapcypridopsis megapodus* is observed. Chironomids *Smittia* and *Parasmittia* appear for the first time and *Cricotopus* and *Phaenopsectra* reach their maximum values. The number of taxa in this zone is the highest of the entire profile. Fluxes of diatoms and chironomids attain their maximum values at around 1300 cal BP.

5. Discussion

5.1. Actual limnology of Laguna Cháltel

Biotic communities indicate oligotrophic conditions for Laguna Cháltel although high total phosphorous concentrations after Vollenweider and Kerekes (1982) would suggest eutrophic to hypertrophic conditions. This has also been observed in other studies of Patagonian lakes (Zolitschka et al., 2006b), A slight increase of pH and oxygen values together with silica depletion in the surface water (Fig. 2c) indicates that some photosynthetic activity took place at the sampling date (2004-03-09).

The observed super-saturation of the lake water with respect to calcium carbonate (Fig. 2c) today should lead to carbonate precipitation. However, TIC percentages in the surface sediments are rather low (Fig. 7) indicating that either precipitation is inhibited, e.g., due to high lake water phosphorous concentrations, or carbonates were dissolved prior, during or after sedimentation. However, idiomorphic carbonate crystals in the sediments (Fig. 3) and on the basaltic rocks above the shoreline document that carbonate precipitation happened in the past. The sigmoidal shapes of carbonate aggregates demonstrate that these are pseudomorphs of calcite after ikaite, so-called glendonites (Swainson and Hammond, 2001; Oehlerich et al., 2013). Ikaite precipitation has been observed during winter season in a comparable Patagonian lake (Laguna Potrok Aike, 52°S) at water temperatures below 7 °C (Oehlerich et al., 2013). In contrast to Laguna Potrok Aike, modern ikaite precipitation at Laguna Cháltel has not yet been observed and it remains unclear if the ikaite precipitated syn-sedimentary or post-depositionally.

Although the installed mooring failed to record water profile information because it drifted ashore, it is likely that surface water temperatures were recorded correctly. Regarding the course of the surface water temperature (Fig. 2b) a striking feature is the almost linear temperature decrease in austral fall that stops abruptly when a temperature of 0.1 °C is reached where a sharp kink followed by a very gentle increase towards ca. 1 °C is observed. This increase is interrupted by a second kink where temperatures start a stepwise increase during austral spring. These two sharp kinks are well developed in most years except for the second kink in 2006. If we hypothesize that these kinks represent the beginning and the end of ice-coverage this would give us an estimate for the annual ice cover duration of 70 to 90 days.

5.2. AMS ^{14}C chronology constrained by paleomagnetic secular variations

The rather low sedimentation rates observed for the Laguna Cháltel record (Fig. 4) are comparable to those encountered e.g. in lakes with

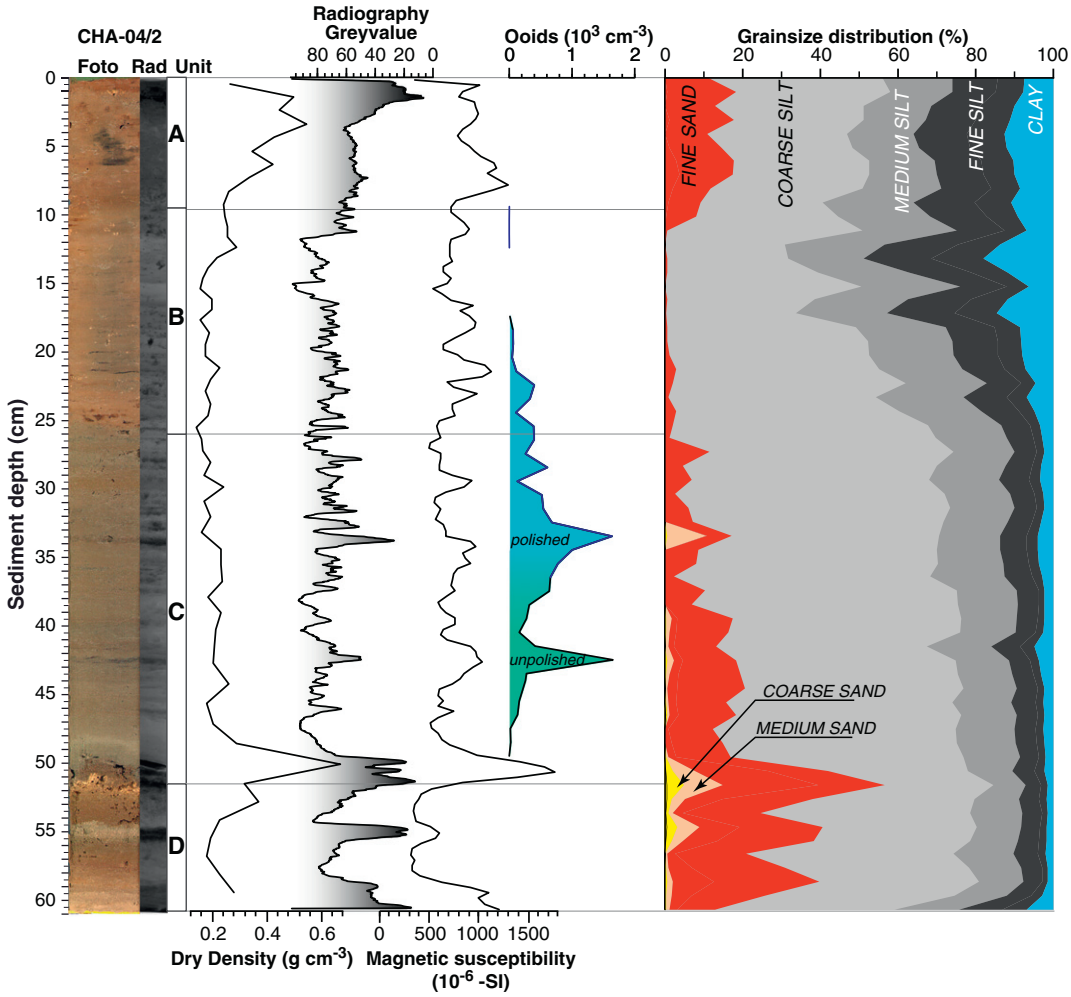

Fig. 6. Physical properties and grain size of Laguna Cháltel sediments displayed next to a core photograph and a radiographic image (Rad). Dry density was determined on core CHA-04/4 and is projected on the CHA-04/2 depth scale. Radiographic gray values, magnetic susceptibility, ooid concentration and grain size distribution (percentages of particles <2 mm) were determined on CHA-04/2.

vegetation free, granitoid catchment in the Chilean Andes (Breuer et al., 2013) or in some Arctic lakes (Guyard et al., 2011). They might be explained by low primary productivity due to the cold and oligotrophic conditions, by a presumably long period of ice cover and by limited clastic input due to erosion-resistant volcanic rocks in the catchment and a lack of major inflows. The deeply incised canyons probably have been formed over a very long time period or under significantly different climatic conditions beyond the time scale of the presented record. Hiatuses in the record as a reason for the apparently low sedimentation rates seem rather unlikely, as indicated by lithological evidence and the stratigraphic consistency of the AMS ^{14}C-dates. Furthermore, there is no evidence for any significant reservoir effect as AMS ^{14}C-dating of living aquatic mosses sampled in March 2004 reveals post-modern ages of AD 1959 or AD 1993 (Table 1) resulting from post-bomb calibration. Additionally, the topmost fine bulk sample taken at 0.5–1.4 cm sediment depth yielded a calibrated age range of 0–286 cal BP. Together with the post-modern age of the living aquatic moss we consider a reservoir effect as highly unlikely. More evidence for the absence of a reservoir effect, for the older sediments of the lake, comes from the fact that ^{14}C-dating of the TIC fraction yielded an age that fits into the stratigraphic order of all other dates that were obtained on bulk organic matter.

Complementary constraints of the AMS ^{14}C-chronology come from paleomagnetic measurements. As shown above, the ChRM is carried by a strong, stable, single component magnetization with MAD values lower than 5°, which are indicative of high-quality directional data (e.g. Stoner and St-Onge, 2007). A comparison between inclination and declination records from Laguna Cháltel plotted on a calendar year time axis together with independently dated Argentinean lacustrine records from lakes Escondido (Gogorza et al., 2002), El Trébol (Irurzún et al., 2006) and Moreno (Gogorza et al., 2000) all located in the Llao-Llao area (41°S, 71.5°W) as well as the record from Laguna Potrok Aike (Lisé-Pronovost et al., 2013) allows the detection of several contemporaneous paleomagnetic features before 2500 cal BP marked with I1–I4 in inclination and D1–D4 in declination (Fig. 5). Especially the declination records from Escondido, Potrok Aike and Laguna Cháltel are in good agreement before 3000 cal BP (Fig. 5). Good agreement is also observed between the inclination records of El Trébol, Moreno and Laguna Cháltel (Fig. 5) although the sediments from Laguna Cháltel seem to record more details since peaks I2 and I3 at Laguna Cháltel appear as one peak in the other two archives. Even a peak at ~4400 cal BP (I1 in Fig. 5) observed in the part of the Laguna Cháltel record which is potentially influenced by the edge-effect is also observed in the other records (Fig. 5).

The agreement between inclination and declination inferred from Laguna Cháltel and the records from the Llao–Llao and Potrok Aike area supports the robustness of our chronology. This is especially true for the time before 2500 cal BP at Laguna Cháltel when the sedimentation rate is higher and hence more details can be observed. Because of the low sedimentation rate after 2500 cal BP and the possible influence

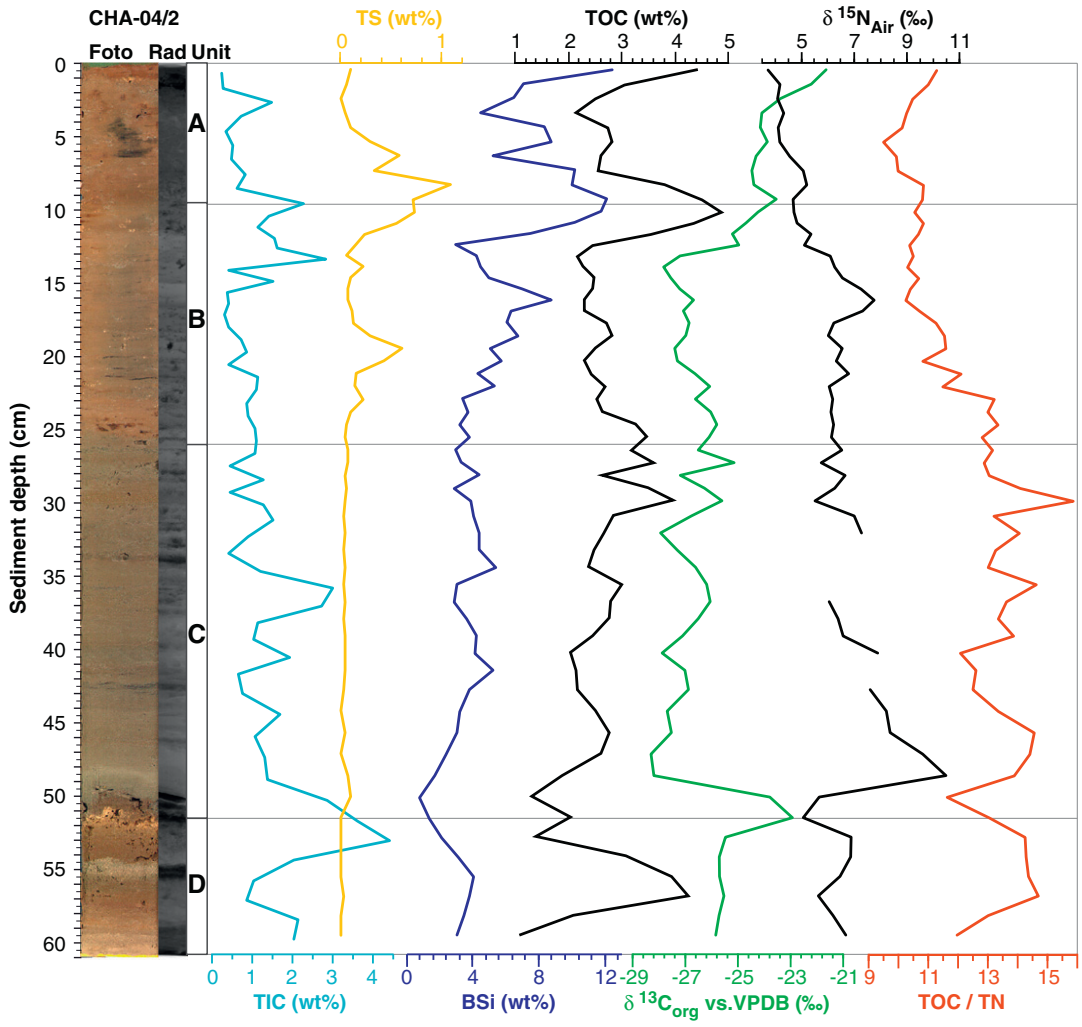

Fig. 7. Organic geochemistry. Chemical properties of Laguna Cháltel sediments displayed next to a core photograph and a radiographic image (Rad). All parameters were determined on core CHA-04/4 and are projected on the CHA-04/2 depth scale. TIC, TS, BSi, TOC values are given as weight percentages (wt.%). $\delta^{13}C_{org}$ and $\delta^{15}N$ in per mil and TOC/TN values are given as ratios.

of an edge effect in the upper part of the core, it is difficult to draw any conclusions for this part of the record. The lower part has a much higher resolution from 4000 to 3000 cal BP and is relatively short (Fig. 5), which might implicate that the expected GAD-value was not reached. In the upper part of the record with lower resolution, smoothing potentially overprinted possible approximations to the GAD.

Hence, the ^{14}C-chronology is constrained by paleomagnetic secular variations which provide new inclination and declination data for the period ~4500–2500 cal BP from an area where only very little paleomagnetic information is available.

5.3. Lake level history

We hypothesize that the detected variations in lithology (e.g. carbonate variety), physical properties, sediment geochemistry and the composition of biological remains (Figs. 6 to 9) all reflect changes that can be used to construct a qualitative lake-level curve of Laguna Cháltel (Fig. 10) for which large uncertainties should be considered.

The division into four lithologic units (Fig. 3) based on core description, closely resembles the biostratigraphic zonation derived from the statistical analysis of bioproxy data (Fig. 9). This underlines the distinctness of changes that occur at the unit boundaries.

Following the lithologic units, four phases of lake-level development are distinguished from the bottom to the top of the core: D) ephemeral lake and desiccation, C) lake re-flooding and shallow lake, B) medium deep lake and A) deep lake.

5.3.1. Unit D (4040–4680 cal BP)

Unit D exhibits TOC rich sediments that alternate with TIC rich layers. TOC/TN ratios above 12 can indicate either higher contributions of macrophytes compared to algae or N-limiting conditions for lacustrine primary production (Mayr et al., 2009). Layers with high Ca/Ti ratios are separated by layers where Fe/Ti and S/Ti are slightly higher probably indicating the occurrence of iron sulfides. The latter may have been formed in the course of bacterial SO_4^{2-}-reduction under anoxic conditions that e.g. develop underneath a salt crust that forms during desiccation periods (Teller et al., 1982). At 55.0 cm (4200 cal BP) high Ca/Ti and high K/Ti values together with increasing Si/Ti and Zr/Ti values point to a minerogenic input of fine sand to silt and clay sized particles which probably originated from the erosion of mudflats surrounding the lake. Increased K-concentrations have been associated to higher clay contents, whereas Zr was found to be enriched in the silt fraction (Cuven et al., 2010; Kylander et al., 2011). However, very low Ti/coh values for most parts of unit D indicate a generally low input of minerogenic particles from the catchment. More positive $\delta^{13}C_{org}$-values at the transition of unit D to C could indicate either a higher photosynthetic production at that time or the prevalence of organic matter (OM) from bicarbonate users (Mayr et al., 2009). Low TOC/TN ratios and

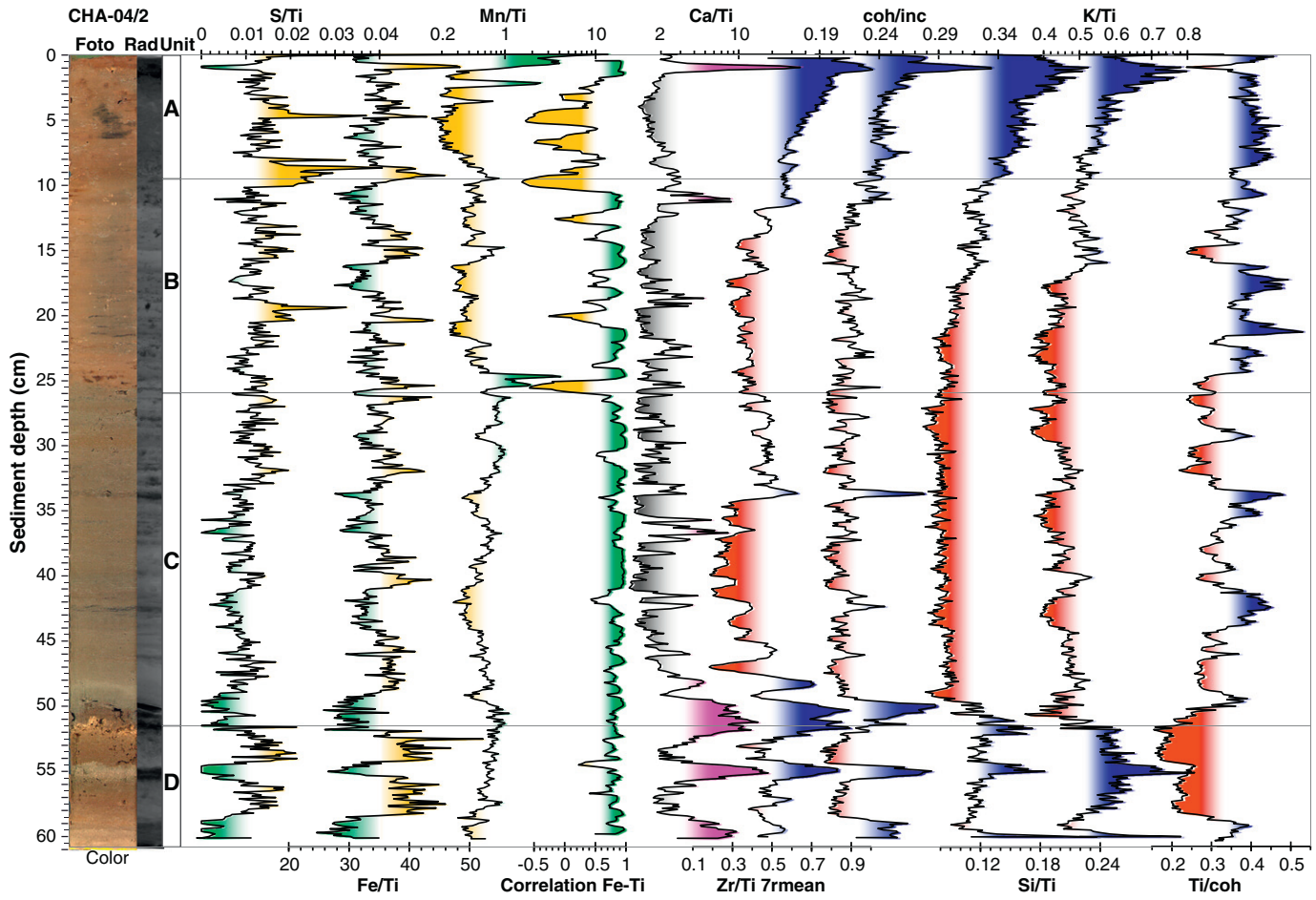

Fig. 8. Inorganic geochemistry. Element ratios determined by XRF-scanning of core CHA-04/2 displayed next to a core photograph and a radiographic image (Rad). Original data is shown for all element ratios except for Zr/Ti, where a 7 point running average is plotted. Element/Ti ratios reflect variations in the mineralogical composition of the detrital matter, Ti/coh ratios reflect variations in the overall input of detrital minerogenic matter and coh/inc ratios reflect general variations of the sediment matrix. The running correlation between Fe and Ti is shown as an indicator of changing redox conditions. Redox indicators are colored from yellow (anoxic) to green (oxic). Proxies reflecting water depth and/or minerogenic input are colored from red (shallow/low input) to blue (deep/high input). Ca/Ti, shown in gray to magenta, does not reflect any of these parameters in the upper three quarters of the record (see text for explanation).

a $\delta^{15}N$ decrease during the $\delta^{13}C_{org}$ maximum strongly argue in favor of cyanobacteria as dominant source of OM at this level (Mayr et al., 2009). The dominance of the ostracod *Limnocythere rionegroensis* indicates salinity values in the mesohaline range (median TDS ≈ 10.000 mg l^{-1}) and Na waters enriched in chlorine and/or sulfate and/or bicarbonate (Cusminsky et al., 2011; Ramón Mercau et al., 2012). A peak of total chironomid and ostracod fluxes (Fig. 9) together with the presence of the littoral chironomid *Polypedilum* evidences low lake levels during this period (Massaferro et al., 2013a). The absence of ooids suggests a frequent occurrence of desiccation phases interrupting shallow water conditions (cf. unit C) that would be necessary for ooid formation.

A very striking feature is the light colored hard crust formed by mineral grains that are cemented by calcite as reflected in high Ca/Ti ratios at 51.5 cm (4040 cal BP) in CHA-04/2. High densities and large coh/inc values characterize this crust and the overlaying dark silty sand layer indicating low porosity and low OM content or a different mineralogical composition (Guyard et al., 2007; Fortin et al., 2013). Within this layer traces of glauberite have been detected which is a mineral typically encountered in very saline environments like dry salt lake beds (Mees et al., 2011) or evaporite deposits (Arakel and Cohen, 1991). Thus this carbonate crust is interpreted as representing a phase when the lake was at least episodically dry that culminated around 4040 cal BP. Today such carbonate crusts are observed in many ephemeral lakes in southeastern Patagonia (e.g. Laguna Bismark, Fig. 1a). In Laguna Cháltel, the basaltic catchment apparently leads to the formation of a Ca and Na rich brine (cf. Fig. 2d) from which glauberite can precipitate when the lake water volume is reduced significantly. Presuming the water chemistry and the lake basin morphology as determined in March 2004 (Figs. 2d, e), a 280-fold evaporative enrichment would be necessary to exceed the solubility of glauberite. A simple linear calculation using the hypsographic curve (Fig. 2e) shows that such enrichment, i.e., a glauberite saturation of 1 or more, would be reached if the lake volume would decrease from today 160×10^6 m^3 to less than 0.57×10^6 m^3, the latter implying a water depth of less than 1 m (Fig. 2e). We therefore suppose that unit D (4680–4040 cal BP) represents a time period when Laguna Cháltel was a playa lake surrounded by mudflats with an ephemeral shallow body of water in the center of the depression. The concentrated brine probably experienced several phases of desiccation which led to precipitation of a carbonate crust with glauberite and the formation of Fe sulfides in the mud underneath. During rainfall events, flooding may have produced layers enriched in minerogenic and organic matter and partial dissolution or erosion of the salt crust. The carbonate crust at 51.5 cm indicates that the last desiccation occurred around 4040 cal BP.

5.3.2. Unit C (3190–4040 cal BP)

At the base of unit C a dark colored, sandy layer was deposited on top of the carbonate crust. The dark color, the roundness of grains together with high values of dry density, coh/inc, Zr/Ti, Ca/Ti and magnetic susceptibility point to a basaltic nature and an eolian transport. Hence, a

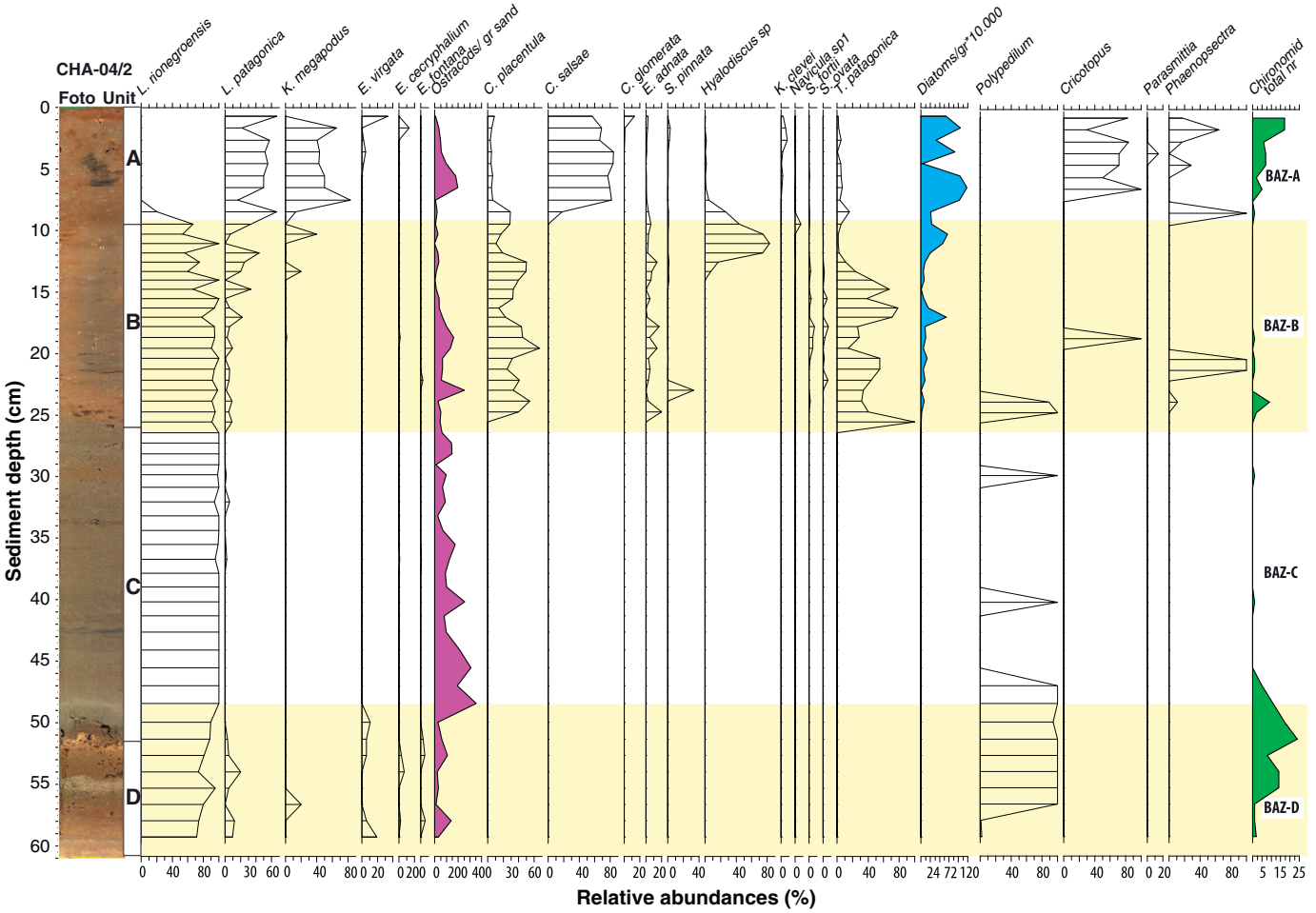

Fig. 9. Bioproxies (% relative abundances) determined on core CHA-04/2. Total numbers of ostracods, diatom, and chironomid, per g sediment are displayed as colored curve. The left column denotes the lithological units as determined during core description. These are very similar to the bioproxy assemblage zones (BAZ) shown in the right column that were determined by optimal partitioning with the program ZONE.

sub-aerial deposition directly on the carbonate crust, in a dry or very shallow lake, or deposition as fluvial input during flood events has to be considered.

After re-flooding of the lake, there is no indication for a renewed massive lake level drop until present day. However, the frequent occurrence of ooids (Figs. 3, 6) in unit C is indicative of a significantly shallower lake than today. Ooids in recent or ancient freshwater environments have only rarely been described (Halley, 1977; Wilkinson et al., 1980; Davaud and Girardclos, 2001). Their presence is commonly associated with shallow and agitated water situations (Flügel, 2010). Ooid sands have been described in the southwestern part of Lake Geneva in well oxygenated, shallow (<5 m) water (Davaud and Girardclos, 2001). In Laguna Cháltel the lowermost ooid peak (Fig. 6) exhibits light colored poorly sorted ooids with rough, dull surfaces indicative of an autochthonous formation without a long transport path (Freeman, 1962). Hence, water depth of Laguna Cháltel at the location of CHA-02/2 probably did not exceed 5 m at that time (3690 cal BP). In contrast, the upper ooid peak shows yellowish, well sorted, ooids with polished surfaces typical for ooids that were transported (Freeman, 1962) and thus are allochthonous with respect to the coring position. Regarding the bathymetry of the lake basin and considering a marked steepening in the curve of the lake surface area (Fig. 2e), the most likely location for ooid formation is the flat areas in the western part of the lake (stippled area in Fig. 1c) that represented a shallow water environment (0–10 m) potentially well suited for the formation of ooidal sands (Fig. 1c). Hence, water depth at the location of CHA-04/2 at that time (3380 cal BP) presumably increased to 5–10 m. Low BSi percentages (<5%), low Si/Ti-ratios (Figs. 6, 7) and the complete absence of diatoms (Fig. 9) point to dissolution of biogenic silica in a saline lake likely due to high pH-values in the water column and in interstitial waters (Barker et al., 1994).

Extreme environmental conditions may also be reflected by the marked dominance of monospecific ostracod assemblages during the entire zone. Monospecific assemblages of *Limnocythere rionegroensis* indicate that the lake hydrochemistry was driven by evaporative conditions. Zamora et al. (2009) interpreted a similar record with predominance of a single ostracod species and absence of diatom remains as evidence of a shallow, saline lake, which is in accordance with the proxy data available for this part of the record. Isolated levels with the chironomid *Polypedilum* and the ostracods *Eucypris* spp., and *Limnocythere patagonica* might be related to episodic pulses of less saline waters (meso-oligohaline). *Polypedilum* is a chironomid that resists heavy drought and its occurrence together with *L. rionegroensis* confirms the hypothesis of a low lake level related to a dry period.

A generally low terrigenous clastic input is indicated by low to intermediate Ti/coh values. Additionally, low Zr/Ti and K/Ti values reveal a reduced input of clay- and silt-sized particles in the lower part of unit C. Together this suggests that mudflats previously surrounding the deepest part of the lake were permanently covered by water and thus not prone to erosion by floods any more as was the case during unit D. Peaks in Ti/coh values at 3400 and 3700 cal BP indicate that ooid deposition was associated with an increased terrigenous clastic input. The

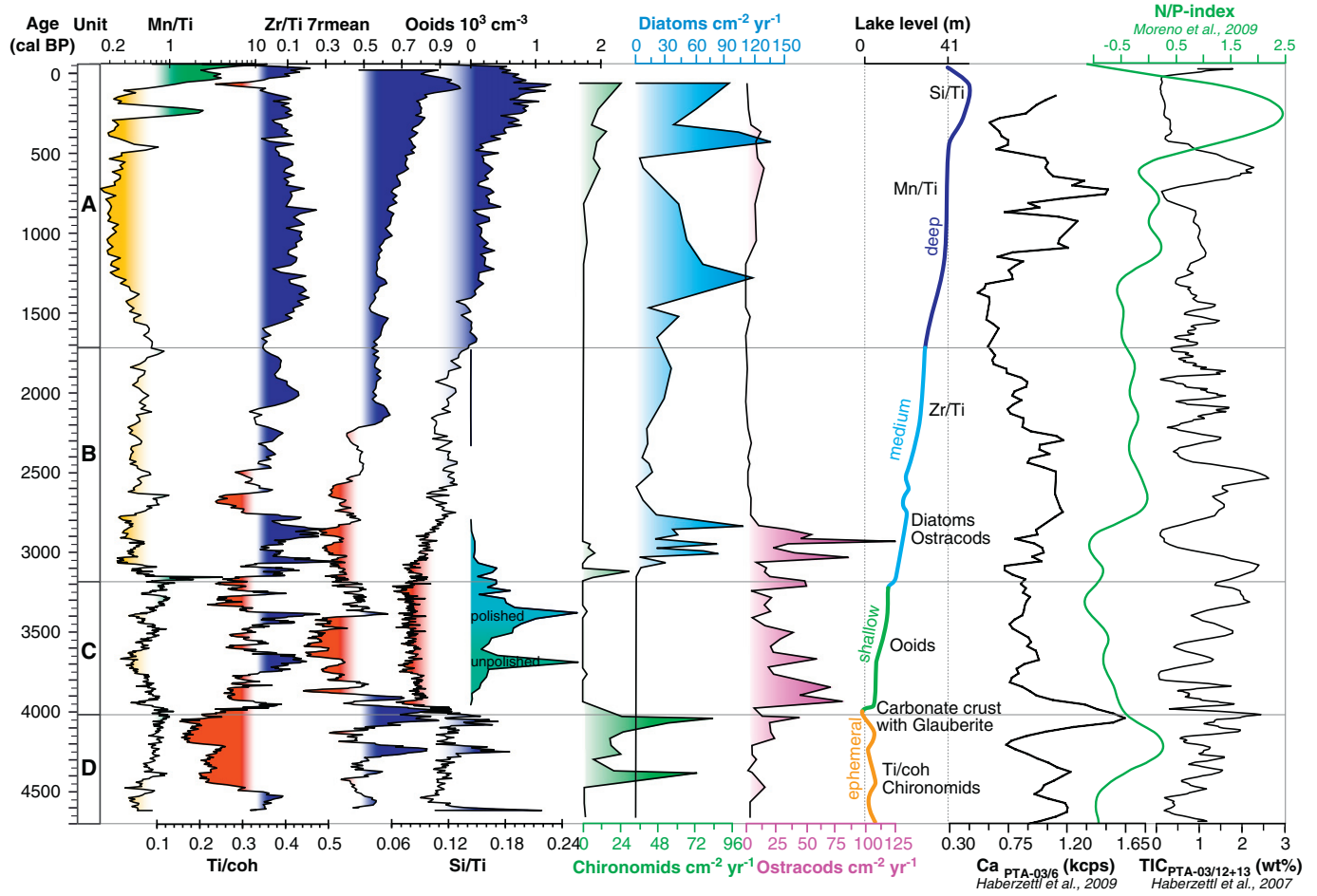

Fig. 10. Comparison of the Laguna Cháltel lake-level history with proxy records from Laguna Potrok Aike (Haberzettl et al., 2007, 2009) and Lago Guanaco (Moreno et al., 2009) (see Fig. 1a for locations). XRF Ca-counts and TIC percentages are shown for Laguna Potrok Aike (PTA) and the *Nothofagus*/*Poaceae* ratio (N/P-index) is displayed for Lago Guanaco. The relative Laguna Cháltel lake-level curve was constructed using different proxies mentioned in the text. Selected proxies are shown to the left of the lake-level-curve. Parameters that were used to derive lake-level information are indicated next to the lake-level curve. The four main lake stages (see text for explanation) are indicated on the left side of the curve and distinguished by different colors.

highest sedimentation rates are recorded in this interval and support this interpretation (Fig. 4). Zr/Ti and coh/inc ratios increase abruptly where the second ooid peak was detected, which indicates that, together with the polished ooids, silt-sized particles were transported to the coring location in the deepest part of the lake. Zr/Ti decreases again afterwards, whereas slightly higher TOC/TN ratios point to an increased input of terrigenous OM shortly after 3400 cal BP. The latter most likely requires increased runoff and thus a further lake-level rise seems likely.

For the entire units D and C, Mn/Ti values vary around their mean and Fe shows a positive correlation with Ti, indicating that it reaches the sediment solely via clastic input from the catchment as it is assumed for the inert Ti. This suggests that the Fe(II)/Fe(III) and Mn(II)/Mn(IV) redox boundaries in the shallow, saline lake of unit C were located in the water column or at the sediment/water interface representing steady-state diagenetic conditions (Kasten et al., 2003) which disable Fe and Mn fixation in the sediment.

5.3.3. Unit B (1720–3190 cal BP)

At the base of unit B, a reddish layer (Fig. 8) with high Mn/Ti values, marks a change in redox conditions at the sediment water interface. Immediately below the Mn/Ti-peak, the positive correlation between Fe and Ti disappears for the first time and Fe/Ti values indicate a slight enrichment of Fe most likely due to reductive processes rather than due to detrital input. Immediately above the Mn/Ti-peak, high Ti/coh values between 2750 and 3150 cal BP indicate an increased terrigenous clastic input. This succession of peaks points to a sudden shift of redox boundaries causing non-steady-state diagenetic conditions (Kasten et al., 2003) and thus leading to a preservation of element peaks in the sediment sequence. The increased accumulation of terrigenous particles as well as the lake-level rise and freshening of the lake probably allowed the fixation of Fe and Mn in the sediment as oxides or hydroxides at this level. This is interpreted as evidence for an initially rapid rise of the lake level, which is also indicated by the occurrence of the highest sedimentation rates around the boundary between units B and C (Fig. 4). Afterwards decreasing Mn/Ti points to steady-state diagenetic conditions again with a redox boundary at the sediment/water interface or in the water column and thus indicates a further rise of the lake level. A peak in S/Ti together with elevated Fe/Ti around 2950 cal BP reflects the presence of Fe sulfides. This suggests the occurrence of bottom water anoxia at least for short time intervals which may be related to reduced lake mixing in response to a higher lake level, less wind and/or extended ice coverage.

The disappearance of ooids and the decrease of fine sand percentages to very low levels also suggest a substantial rise of the lake level after 3200 cal BP. In the upper part of unit B the starting increase of first silt and then clay percentages (Fig. 6) as also reflected by increasing Zr/Ti and K/Ti (Fig. 8) most likely reflect increased fluvial minerogenic input and are interpreted as a further lake-level rise(Fig. 10). At the

same time, the appearance of the ostracod *Limnocythere patagonica* indicates a gradual decrease in salinity (meso-oligohaline) also related to an increase in the lake water level probably driven by moister climate conditions. Evaporative conditions gradually decrease, and the lake water probably became Na–Ca–Mg dominated. During this period, the presence of the diatoms *Thalassiosira patagonica* (planktonic) and *Cocconeis placentula* var. *euglypta* (epiphytic) also indicates a less saline environment with abundant shallow-water macrophytes. TOC/TN values start to decrease synchronically with the abrupt appearance of diatoms indicating autochthonous sources of organic matter. A trend towards higher Si/Ti ratios and higher BSi percentages starts slightly later (3050 cal BP), which is related to a better preservation of diatoms due to pH reduction and freshening of the lake water. The increase of algal activity i. e. enhanced photosynthesis may have promoted a shift towards more alkaline conditions. Between 2200 and 1630 cal BP, the appearance and dominance of *Hyalodiscus* sp. and the decrease of *C. placentula* var. *euglypta* and *T. patagonica* indicate even lower salinity than during the initial phase of unit B suggesting a further increase of the lake level. The high abundances of the ostracod *L. patagonica* by that time support this interpretation. In addition, a trend towards more positive $\delta^{13}C_{org}$-values in conjunction with no marked change in the TOC/TN ratios either indicates increasing lake-internal primary production in the upper part of unit B or increased proportions of cyanobacterial OM (after 2200 cal BP). The latter is supported by lower $\delta^{15}N$ values (Mayr et al., 2009). No chironomids were found in unit B, which may be related to food availability for profundal communities, due to the rise of the lake level and hypolimnetic anoxic conditions (Verbruggen et al., 2011).

Instead of ooids, sigmoidal and star shaped carbonate crystals appear scattered in unit B. Hence, the Ca/Ti profile mainly reflects the scattered occurrence of these syn- or post-depositional carbonate crystals in the sediments (Fig. 8). Therefore, we refrain from a detailed paleoenvironmental interpretation of the Ca/Ti profile in units B and A. Star-like crystal shapes argue for pseudomorphs of calcite after ikaite (Fig. 3) and indicate a formation at water temperatures below 7 °C (Oehlerich et al., 2013). Such morphologies were interpreted as synsedimentary ikaites precipitated on the sediment surface in Oligocene lacustrine travertine (Larsen, 1994). The pseudomorphs after ikaite that occur in the upper part of the sediment profile (unit A and top of unit B) more and more have the shape of rice grains and star-shaped aggregates disappear. Such pseudomorph shapes were attributed to formation near the sediment–water interface in Oligocene tuffaceous lake beds (Larsen, 1994). However, at Laguna Potrok Aike (230 km to the south, Fig. 1a) ikaite crystals were growing attached to aquatic macrophytes as well as on abiotic surfaces (e.g., the mooring rope) in the water column (Oehlerich et al., 2013).

At the transition of unit B to unit A, around 1720 cal BP, high TOC and BSi values together with more positive $\delta^{13}C_{org}$-values indicate a high primary productivity. Together with a lake-level rise, this may have led to bottom water anoxia with Fe sulfide deposition, as supported by increased S percentages, high S/Ti and Fe/Ti in the lower part of unit A (Fig. 8).

5.3.4. Unit A (−50–1720 cal BP)

The disappearance of star-shaped carbonate crystals in unit A suggests that conditions in the topmost 9 cm of the sediment largely did not support ikaite formation. This might be attributed to unsuitable pore/lake water chemistry or rapid decay of ikaite crystals after their formation as observed presently at Laguna Potrok Aike (Oehlerich et al., 2013). Increasing sediment densities (Fig. 6), the occurrence of fine sand (Fig. 6), as well as higher Ti/coh, Zr/Ti, K/Ti and coh/inc values (Fig. 8) reflect an increase of minerogenic input from the catchment relative to biogenic and carbonate sediment components for this period of low sedimentation rates (Fig. 4). The interval with black laminations in the middle part of unit A is considered to represent conditions with the most pronounced lake bottom water anoxia. Very low TIC percentages, lowest TOC/TN ratios and low total accumulation rates point to low-salinity conditions. At the same time, the increase of fine sand percentages (Fig. 3) and relatively high magnetic susceptibility (Fig. 6) may reflect an increased amount of particles originating from the basaltic catchment and reaching the coring position e.g. by fluvial or eolian input directly into the water body of the lake or indirectly onto a persisting ice cover. Thus the lake level during this interval probably was at its maximum of approximately 10 m above the AD 2004 level as deduced from exposed lacustrine sediments and carbonate precipitates on the basaltic rocks. Moreover, elevated S percentages and S/Ti values coinciding with negative Fe to Ti correlation and slight maxima in Fe/Ti values (Fig. 8) suggest Fe sulfide formation which would indicate a more frequent occurrence of bottom water anoxia. This is supported by a strong depletion of Mn (low Mn/Ti values, Figs. 8, 10), which indicates that Mn was not fixed in the sediment by oxidation. We hypothesize that during this interval phases of inhibited lake mixing i.e., reduced water circulation due to a deeper lake, less wind, lake stratification or elongated periods of ice cover occurred.

This interval started around 1720 cal BP and culminated with the lowest Mn/Ti values of the record at 730 cal BP (AD 1220), i.e. during Late Medieval times. Two peaks towards high Mn/Ti values at 270 cal BP (AD 1680) and 440 cal BP (AD 1510), hence during the Little Ice Age (Fig. 10) may represent phases with lake circulation when the bottom sediments were oxygenated for a short period of time and became anoxic shortly afterwards again probably due to a long period of ice cover. Strongly increasing Mn/Ti values after 100 cal BP (AD 1850) indicate an oxygenation of the bottom sediment with increasing preservation of Mn as oxides. This reflects the present position of the redox boundary probably associated to a recent decrease of the lake level in combination with bottom water oxygenation due to more frequent lake circulation as it is observed today (Fig. 2c). However, the three most recent Fe/Ti maxima occur during a long interval of very low Mn/Ti values, indicating that bottom water redox conditions in the intervals in between the Fe/Ti maxima did not recover but still were anoxic. Because the highest Si/Ti values are concomitant with high K/Ti and Zr/Ti between 0 and 400 cal BP (Fig. 10) while BSi values and diatom concentrations are rather low, Si/Ti in this interval probably reflects both, an increased minerogenic input of silt and clay and an increased primary production.

Bioproxies support the above interpretations because at the beginning of Zone A, *Limnocythere rionegroensis* disappears and is completely replaced by *Kapcypridopsis megapodus* and *Limnocythere patagonica*. The latter is a stenohaline freshwater taxon, typical for alkaline (bicarbonate dominated) waters with low $(HCO_3^- + CO_3^{2-})/Ca^{2+}$ ratios, salinities generally below 500 mg l^{-1} TDS (median TDS ≈ 200 mg l^{-1}), and significant carbonate enrichment (Ramón Mercau et al., 2012). This replacement in the ostracod assemblage points to a major shift in the lake hydrochemistry towards HCO_3^-, Ca–Na–Mg dominated waters and salinity an order of magnitude lower than in previous zones. The diatom *Hyalodiscus* sp. is replaced by *Cyclostephanos salsae*. At the same time, *Thalassiosira patagonica* and *Cocconeis placentula* var. *euglypta* decrease. The presence of the littoral and semi-terrestrial chironomids *Smittia* and *Parasmittia*, littoral *Cricotopus* and more profundal *Phaenopsectra*, together with the presence of subaereal diatoms suggests the expansion of littoral habitats following a lake level rise and increased turbulence and sediment transport to the center of the lake. The high turbulence and lake internal transport may be related to wind intensity and increased precipitation. This period is characterized by a high biodiversity and autochthonous origin of the OM as deduced from relatively lower TOC/TN ratios.

In summary, we hypothesize a development as visualized in the lake-level curve (Fig. 10). Prior to 4040 cal BP, Laguna Cháltel was an ephemeral, saline lake surrounded by mudflats. Re-flooding of the lake occurred after 4040 cal BP followed by a period with a shallow (max. 10 m), but permanent, mesohaline lake until 3200 cal BP. Thereafter, a further lake-level rise and freshening occurred that was

fast in the initial stage until 2800 cal BP and slowed down until 1720 cal BP. This period was followed by a faster lake-level rise until ca. 1200 cal BP and a stagnating lake level with bottom water anoxia until ca. 500 cal BP. The highest lake level probably was reached around 60 cal BP followed by a decrease to present day lake levels.

5.4. Lake-level development of Laguna Cháltel compared to other archives

The inferred lake-level variations at Laguna Cháltel are an expression of changes in the hydrological balance of the lake which mainly reflects the evaporation-to-inflow ratio. This in turn is controlled by a multitude of meteorological and catchment factors like e.g. precipitation, wind speed, relative humidity, ground-water supply, catchment size, lake ice coverage and others (Ohlendorf et al., 2013). Because of to the remoteness of Laguna Cháltel, most of these factors are unknown and the direct inference of past meteorological conditions from changes in the hydrological balance is not advisable. However, Ohlendorf et al. (2013) have shown that, on short time scales, lake-level fluctuations at Laguna Potrok Aike (Fig. 1a) are mainly driven by changes in relative humidity, precipitation, temperature, wind strength and wind direction which in turn are controlled by variations in the strength of the SWW. With this assumption we compare our lake-level reconstruction for Laguna Cháltel to other paleohydrological evidences from the southeastern Patagonian dry steppe (Fig. 10). For instance, increasing precipitation was reconstructed for 4400, 2900, 1300 and 570 cal BP (Moreno et al., 2009) at Lago Guanaco using the *Nothofagus*/*Poaceae* ratio as an indicator of precipitation related to the SWW-intensity (Moreno et al., 2010). Lago Guanaco is located further to the west (Fig. 1a) at the modern forest-steppe ecotone and reflects strengthened SWWs as periods with increased precipitation. This is in contrast to sites located further to the east which record increased SWW-intensity as decreases in precipitation (Garreaud et al., 2013). E.g. in Laguna Potrok Aike, the time interval 4000–4700 cal BP corresponds to a period, when a pronounced regressional phase was inferred from high TIC concentrations (Fig. 10) and from regressive shorelines visible on seismic profiles (Anselmetti et al., 2009; Haberzettl et al., 2009). This is corroborated by diatom and chironomid data (Massaferro et al., 2013a) and pollen-based reconstruction of paleo-precipitation (Schäbitz et al., 2013) and was also ascribed to strengthened SWW, which at this site in the eastern steppe is associated to a reduction in precipitation and/or an increase in evaporation (Mayr et al., 2007). The suggested desiccation of a pre-existing ephemeral playa lake of Laguna Cháltel, around 4040 cal BP (Fig. 10) would fit with these regional reconstructions. However, lake-level reconstructions of Lago Cardiel indicate that after an early Holocene high stand of +55 m the lake level never dropped significantly below the modern level (Gilli et al., 2005a), although between 3000 and 5000 cal BP lake-level data is not available. At Laguna Potrok Aike, the dry period around 4000 cal BP is only a dry episode in a general trend towards a less negative water balance that started around 7300 cal BP. Actually, much drier conditions were observed before with the most severe dry period occurring between 7300 and 8700 cal BP (Haberzettl et al., 2007) coinciding with strongest Holocene SWW influence (Mayr et al., 2007). Hence, assuming a similar development for Laguna Cháltel would imply that the threshold for lake-desiccation was reached for the last time around 4040 cal BP. Longer and more severe desiccation phases probably occurred prior to this date. After this marked dry event the sedimentological, geochemical and biological evidences of the Laguna Cháltel record suggest that re-flooding of the lake took place and the subsequent lake-level increase was persistent and not interrupted by desiccation events until present day. This is in accordance with other reconstructions from this area (Cross et al., 2000; Haberzettl et al., 2007) where the change towards moister conditions is ascribed to a northward shift of the SWW. For Laguna Cháltel, a northerly shift of the SWW most likely would imply a higher probability for air masses of Atlantic origin to reach the lake (Mayr et al., 2007). In addition reduced SWW intensity at Laguna Cháltel also would lead to less evaporation and presumably extend the period of ice coverage. Both factors would contribute to a positive hydrological balance of the lake and thus result in a lake-level increase.

Given the age uncertainty of ±200 years for the 4040 cal BP date (Fig. 4, Table 1), we hypothesize that the observed desiccation event followed by a re-flooding of the lake maybe linked to the global environmental changes that are associated to the 4.2 ka event. The occurrence of a climatic event around 4200 cal BP has been discussed by several authors (Cullen et al., 2000; Roberts et al., 2011; Ülgen et al., 2012). Namely, the collapse of the Old World urban civilizations in the Middle East was ascribed to a marked increase in aridity and severe drought around 4200 cal BP (Arz et al., 2006). Although the detection of a climate signal at 4200 cal BP in Europe, parts of Africa, Asia, North America and South America points to its global significance (Marchant and Hooghiemstra, 2004; Booth et al., 2005), origin and regional impacts of this event are still debated (Roland et al., 2014). Since the Laguna Cháltel record below the desiccation event at 4040 cal BP reaches back in time for only 700 more years with a playa lake facies, a link to the 4.2 ka event is not unequivocal. Although the lake bathymetry (steep walls, flat bottom) and the deeply incised canyons in the catchment point to a considerable age of the lake, it cannot be completely ruled out that the playa lake phase represents the start of lacustrine sedimentation during an initial lake phase.

Also the increase of the Laguna Cháltel lake level in several steps, around 3200 and 1600 cal BP is broadly synchronous to the record e.g. of Lago Guanaco (Fig. 10; Moreno et al., 2009). For instance, the time when highest sedimentation rates are observed at Laguna Cháltel (2800–3200 cal BP) corresponds to a cold phase with significantly lower precipitation in a speleothem record on the western side of the Andes (Schimpf et al., 2011). A global cooling around 2800 cal BP due to reduced solar irradiance was proposed by van Geel et al. (2000) which presumably would have led to a northward movement of the SWW. For the latitude of Laguna Cháltel this would imply a SWW weakening with the consequences of a) less evaporation due to lower wind speeds and lower air temperatures (prolonged lake ice coverage) and/or b) more precipitation due to increased easterly flow. Both factors could explain the observed increase in sedimentation rates probably due to enhanced clastic input. The greatest water depth at Laguna Cháltel supposedly occurred during the LIA (60–200 cal BP) as was also observed for Laguna Potrok Aike (Haberzettl et al., 2005). However, stagnating lake levels in Laguna Cháltel during later parts of the Medieval Period (500–1000 cal BP) rather resemble the pattern observed at Lago Guanaco (Moreno et al., 2009). The trends observed in the Laguna Cháltel record might be comparable to observations from Laguna Las Vizcachas, a cirque lake ca. 80 km to the SSW of Laguna Cháltel (Fey et al., 2009). This record indicates increased precipitation during Late Medieval times, which was ascribed to higher SWW-intensity whereas lower SWW-intensity during the LIA led to less precipitation. The positive hydrologic balance in Laguna Potrok Aike and Lago Guanaco was likely associated with increased rainfall from easterly directions that can reach these lowland sites during phases of weaker SWW like in the LIA. In contrast, Fey et al. (2009) suggested that precipitation associated to easterly airflow cannot reach the high-altitude site of Laguna Las Vizcachas as frequently as the lowland sites. Hence, the hydrologic balance at this high-altitude site might reflect to a certain extent that of southwestern Patagonia, where strong SWW are associated with higher precipitation and not with higher evaporation caused by a strong "foehn"-like effect (Ohlendorf et al., 2013). Due to its slightly more westerly location and its higher altitudinal position on the Pampa Alta plateau, Laguna Cháltel might represent a site where, apart from SWW forcing, local climate fluctuations are more important (Garreaud et al., 2013). Considering the outlined hydrological development in the southeastern Patagonian realm and conceding imprecisions for the chronologies of all discussed records, as well as respecting differences in the altitudes of the different sites, reveals the SWW as the dominant hydrological control mechanism.

6. Conclusions

Our interdisciplinary study carried out at Laguna Cháltel revealed several remarkable features of this remote lake. Today, the lake can be classified as an oligotrophic system with low primary production in spite of high lake water phosphorus concentration as it has been observed in previous studies from Patagonia (e.g. Zolitschka et al., 2006b; Diaz et al., 2007). The lake water is characterized by supersaturation with respect to calcium carbonate, although no carbonates are encountered in the basaltic catchment. While TIC percentages are low in the surface sediments, pseudomorphs of calcite after ikaite developed as star-shaped and rice-grain-shaped crystals presumably on the sediment surface and possibly also in the sediment as well as on formerly water covered basaltic boulders up to 10 m above the present day lake level. A better understanding of the carbonate system in Laguna Cháltel thus seems to be one of the key issues for a consolidated interpretation of its sediment record. The occurrence of a glauberite-bearing carbonate crust around 4040 cal BP is interpreted as a lake-desiccation event. Admitting chronological uncertainties, we suggest that this event may be contemporaneous to the globally recognized 4.2 ka event (Booth et al., 2005) that had a severe impact on ancient civilizations elsewhere. In the Laguna Cháltel record, this event is reflected by a lake desiccation that was followed by a shift towards a positive water balance. This initially led to an 800-year long period with a shallow lake and culminated in a lake-level high-stand at the end of the LIA. The former was reconstructed based on the occurrence of ooids in the sediments immediately above the desiccation horizon and is supported by bioproxies and geochemical evidence. This is one of the rare cases where ooids are encountered in a lacustrine environment. We thus conclude that the occurrence of different carbonate phases and morphologies is a unique feature of the Laguna Cháltel record.

The reconstructed mid- to Late Holocene lake-level evolution of Laguna Cháltel is in general agreement with other records from southeastern Patagonia and thus underlines the important role of SWW-variations for the regional hydrological balance of the southeastern steppe (Mayr et al., 2013; Zolitschka et al., 2013). However, inconsistencies of the lake-level reconstruction with the conceptual model of SWW control on local hydrology point to a more complex relationship. The elevated location could entail mesoscale meteorological processes that may influence the local hydrological balance namely the amount of precipitation at the lake. Moreover, the occurrence of lake ice cover during 2 to 3 month each year is suggested by surface water temperature monitoring of Laguna Cháltel and certainly also has an impact on lake evaporation rates.

Finally, the question whether the carbonate crust close to the bottom of the core represents a single desiccation event around 4040 cal BP or is only the last of more severe desiccations that occurred before this date, cannot be determined based on the existing short core that reaches back to 4700 cal BP. A longer core penetrating into strata covering the entire Holocene would shed more light on the singularity of the observed desiccation event.

Acknowledgments

The authors thank Sabine Stahl, Benjamin Bünning, Tim Haarmann, Barbara Kück and Sabine Wrocklage for assistance with sampling and geochemical analyses as well as Holger Wissel and Werner Laumer for technical assistance with stable isotope analyses. Michael Lindner and Dominik Tallarek are acknowledged for pollen preparation. We thank Catalina Gebhardt for helping hands in the field, assistance during grain size analyses and for helpful discussions. The help of Cristina Recasens during fieldwork is gratefully acknowledged. We are much obliged to Cornelia Dasenbrock for sieving and counting the ooids. For providing technical equipment and know-how at the ODP/IODP Bremen Core Repository, we would like to thank Walter Hale, Heike Pfletschinger, Ursula Röhl and Alexius Wülbers. We are much obliged to Thomas Frederichs and Christian Hilgenfeldt for access to their magnetic measuring bench. Christoph Vogt is gratefully acknowledged for performing XRD-analyses. We thank the late Cristóbal Kennard, Capt. Jorge D. Moreteau and the staff of INTA, Río Gallegos, for their tireless assistance in organizing the logistics of the field work. The 'puma hunter' Ávila is acknowledged for horseback transport of equipment to the lake. Torsten Haberzettl was supported by a postdoctoral fellowship provided by Le Fonds québécois de la recherche sur la nature et les technologies (FQRNT). Guillaume St-Onge was supported by a NSERC (Natural Sciences and Engineering Research Council of Canada) discovery grant and Canadian Foundation for Innovation (CFI) grants for the acquisition and operation of the cryogenic magnetometer. This is a contribution to the project "South Argentinean Lake Sediment Archives and modeling" (SALSA) within the framework of the German Climate Research Program DEKLIM (grants 01 LD 0034 and 0035) of the German Federal Ministry of Education and Research (BMBF). Additional financial support was provided by the German Science Foundation (DFG) in the framework of the Priority Program 'ICDP' (grants ZO 102/5-1, ZO 102/5-2, and ZO 102/5-3 and MA 4235-1 and MA 4235-2).

Appendix A. Supplementary data

Supplementary data associated with this article can be found in the online version, at http://dx.doi.org/10.1016/j.palaeo.2014.06.030. These data include Google maps of the most important areas described in this article.

References

Anselmetti, F.S., Ariztegui, D., Batist, M.D., Gebhardt, A.C., Haberzettl, T., Niessen, F., Ohlendorf, C., Zolitschka, B., 2009. Environmental history of southern Patagonia unravelled by the seismic stratigraphy of Laguna Potrok Aike. Sedimentology 56, 873–892.

Arakel, A.V., Cohen, A., 1991. Deposition and early diagenesis of playa glauberite in the Karinga Creek drainage system, Northern Territory, Australia. Sediment. Geol. 70, 41–59.

Ariztegui, D., Bosch, P., Davaud, E., 2007. Dominant ENSO frequencies during the Little Ice Age in Northern Patagonia: the varved record of proglacial Lago Frias, Argentina. Quat. Int. 161, 46–55.

Arz, H.W., Lamy, F., Pätzold, J., 2006. A pronounced dry event recorded around 4.2 ka in brine sediments from the northern Red Sea. Quat. Res. 66, 432.

Barker, P., Fontes, J.-C., Gasse, F., Druart, J.-C., 1994. Experimental dissolution of diatom silica in concentrated salt solutions and implications for paleoenvironmental reconstruction. Limnol. Oceanogr. 39, 99–110.

Battarbee, E.W., 1986. Diatom analysis. In: Berglund, B.E. (Ed.), Handbook of Holocene Palaeoecology and Palaeohydrology. J. Wiley & Sons, New York, pp. 527–570.

Bennett, K.D., 1996. Determination of the number of zones in a biostratigraphical sequence. New Phytol. 132, 155–170.

Berman, A.L., Silvestri, G., Compagnucci, R., 2012. Eastern Patagonia seasonal precipitation: influence of southern hemisphere circulation and links with subtropical South American precipitation. J. Clim. 25, 6781–6795.

Birks, H.J.B., Gordon, A.D., 1985. Numerical Methods in Quaternary Pollen Analysis. Academic Press, London.

Booth, R.K., Jackson, S.T., Forman, S.L., Kutzbach, J.E., Bettis, E.A., Kreigs, J., Wright, D.K., 2005. A severe centennial-scale drought in midcontinental North America 4200 years ago and apparent global linkages. The Holocene 15, 321–328.

Breuer, S., Kilian, R., Baeza, O., Lamy, F., Arz, H., 2013. Holocene denudation rates from the superhumid southernmost Chilean Patagonian Andes (53°S) deduced from lake sediment budgets. Geomorphology 187, 135–152.

Corbella, H., Lara, L.E., 2008. Late Cenozoic Quaternary volcanism in Patagonia and Tierra del Fuego. In: Rabassa, J. (Ed.), The Late Cenozoic of Patagonia and Tierra del Fuego. Elsevier, pp. 95–119.

Cranston, P.S., 2000. Electronic Guide to the Chironomidae of Australia. http://entomology.ucdavis.edu/chiropage/index.html2012.

Cross, S.L., Baker, P.A., Seltzer, G.O., Fritz, S.C., Dunbar, R.B., 2000. A new estimate of the Holocene lowstand level of Lake Titicaca, central Andes, and implications for tropical palaeohydrology. The Holocene 10, 21–32.

Croudace, I.W., Rindby, A., Rothwell, R.G., 2006. ITRAX: description and evaluation of a new multi-function X-ray core scanner. In: Rothwell, R.G. (Ed.), New Techniques in Sediment Core Analysis. Geological Society of London Special Publications, London, pp. 51–63.

Cullen, H.M., deMenocal, P.B., Hemming, S., Hemming, G., Brown, F.H., Guilderson, T., Sirocko, F., 2000. Climate change and the collapse of the Akkadian empire: evidence from the deep sea. Geology 28, 379–382.

Cusminsky, G.C., Pérez, P.A., Schwalb, A., Whatley, R., 2005. Recent lacustrine ostracods from Patagonia, Argentina. Rev. Esp. Micropaleontol. 37, 431–450.

Cusminsky, G., Schwalb, A., Pérez, A.P., Pineda, D., Viehberg, F., Whatley, R., Markgraf, V., Gilli, A., Ariztegui, D., Anselmetti, F.S., 2011. Late quaternary environmental changes in Patagonia as inferred from lacustrine fossil and extant ostracods. Biol. J. Linn. Soc. 103, 397–408.

Cuven, S., Francus, P., Lamoureux, S.F., 2010. Estimation of grain size variability with micro X-ray fluorescence in laminated lacustrine sediments, Cape Bounty, Canadian High Arctic. J. Paleolimnol. 44, 803–817.

Davaud, E., Girardclos, S., 2001. Recent freshwater ooids and oncoids from Western Lake Geneva (Switzerland): indications of a common organically mediated origin. J. Sediment. Res. 71, 423–429.

de Porras, M.E., Mancini, M.V., Prieto, A.R., 2011. Modern pollen analysis in caves at the Patagonian steppe, Argentina. Rev. Palaeobot. Palynol. 166, 335–343.

Diaz, M., Pedrozo, F., Reynolds, C., Temporetti, P., 2007. Chemical composition and the nitrogen-regulated trophic state of Patagonian lakes. Limnologica 37, 17–27.

D'Orazio, M., Innocenti, F., Manetti, P., Haller, M.J., 2004. Cenozoic back-arc magmatism of the southern extra-Andean Patagonia (44° 30′–52° S): a review of geochemical data and geodynamic interpretations. Rev. Asoc. Geol. Argent. 59, 525–538.

Fey, M., Korr, C., Maidana, N.I., Carrevedo, M.L., Corbella, H., Dietrich, S., Haberzettl, T., Kuhn, G., Lücke, A., Mayr, C., Ohlendorf, C., Paez, M.M., Quintana, F.A., Schäbitz, F., Zolitschka, B., 2009. Palaeoenvironmental changes during the last 1600 years inferred from the sediment record of a cirque lake in southern Patagonia (Laguna Las Vizcachas, Argentina). Palaeogeogr. Palaeoclimatol. Palaeoecol. 281, 363–375.

Fletcher, M.-S., Moreno, P.I., 2011. Have the Southern Westerlies changed in a zonally symmetric manner over the last 14,000 years? A hemisphere-wide take on a controversial problem. Quat. Int. 253, 32–46.

Flügel, E., 2010. Microfacies of Carbonate Rocks. Analysis, Interpretation and Application, 2 edition. Springer.

Fortin, D., Francus, P., Gebhardt, A.C., Hahn, A., Kliem, P., Lisé-Pronovost, A., Roychowdhury, R., Labrie, J., St-Onge, G., 2013. Destructive and non-destructive density determination: method comparison and evaluation from the Laguna Potrok Aike sedimentary record. Quat. Sci. Rev. 71, 147–153.

Freeman, T., 1962. Quiet water oolites from Laguna Madre, Texas. J. Sediment. Res. 32, 475–483.

Funk, J.A., von Dobeneck, T., Reitz, A., 2004. Integrated rock magnetic and geochemical quantification of redoxomorphic iron mineral diagenesis in Late Quaternary sediments from the Equatorial Atlantic. In: Wefer, G., Mulitza, S., Ratmeyer, V. (Eds.), The South Atlantic in the Late Quaternary: Reconstruction of Material Budgets and Current Systems. Springer-Verlag, pp. 237–260.

Garreaud, R.D., Vuille, M., Compagnucci, R., Marengo, J., 2009. Present-day South American climate. Palaeogeogr. Palaeoclimatol. Palaeoecol. 281, 180–195.

Garreaud, R., Lopez, P., Minvielle, M., Rojas, M., 2013. Large-scale control on the Patagonian climate. J. Clim. 26, 215–230.

Gilli, A., Anselmetti, F.S., Ariztegui, D., Beres, M., McKenzie, J.A., Markgraf, V., 2005a. Seismic stratigraphy, buried beach ridges and contourite drifts: the Late Quaternary history of the closed Lago Cardiel basin, Argentina (49°S). Sedimentology 52, 1–23.

Gilli, A., Ariztegui, D., Anselmetti, F.S., McKenzie, J.A., Markgraf, V., Hajdas, I., McCulloch, R. D., 2005b. Mid-Holocene strengthening of the Southern Westerlies in South America — sedimentological evidences from Lago Cardiel, Argentina (49°S). Glob. Planet. Chang. 49, 75–93.

Gogorza, C.S.G., Sinito, A.M., Vilas, J.F., Creer, K.M., Nuñez, H., 2000. Geomagnetic secular variations over the last 6500 years as recorded by sediments from the lakes of south Argentina. Geophys. J. Int. 143, 787–798.

Gogorza, C.S.G., Sinito, A.M., Lirio, J.M., Nuñez, H., Chaparro, M., Vilas, J.F., 2002. Paleosecular variations 0–19,000 years recorded by sediments from Escondido Lake (Argentina). Phys. Earth Planet. Inter. 133, 35–55.

Gogorza, C.S.G., Irurzun, M.A., Sinito, A.M., Lisé-Pronovost, A., St-Onge, G., Haberzettl, T., Ohlendorf, C., Kastner, S., Zolitschka, B., 2012. High-resolution paleomagnetic records from Laguna Potrok Aike (Patagonia, Argentina) for the last 16,000 years. Geochem. Geophys. Geosyst. 13, 1–18.

Guyard, H., Chapron, E., St-Onge, G., Anselmetti, F.S., Arnaud, F., Magand, O., Francus, P., Mélières, M.-A., 2007. High-altitude varve records of abrupt environmental changes and mining activity over the last 4000 years in the Western French Alps (Lake Bramant, Grandes Rousses Massif). Quat. Sci. Rev. 26, 2644–2660.

Guyard, H., St-Onge, G., Pienitz, R., Francus, P., Zolitschka, B., Clarke, G.K.C., Hausmann, S., Salonen, V.-P., Lajeunesse, P., Ledoux, G.g, Lamothe, M., 2011. New insights into Late Pleistocene glacial and postglacial history of northernmost Ungava (Canada) from Pingualuit Crater Lake sediments. Quat. Sci. Rev. 30, 3892–3907.

Haberzettl, T., Fey, M., Lücke, A., Maidana, N., Mayr, C., Ohlendorf, C., Schäbitz, F., Schleser, G.H., Wille, M., Zolitschka, B., 2005. Climatically induced lake level changes during the last two millennia as reflected in sediments of Laguna Potrok Aike, southern Patagonia (Santa Cruz, Argentina). J. Paleolimnol. 33, 283–302.

Haberzettl, T., Corbella, H., Fey, M., Janssen, S., Lücke, A., Mayr, C., Ohlendorf, C., Schäbitz, F., Schleser, G.H., Wille, M., Wulf, S., Zolitschka, B., 2007. Lateglacial and Holocene wet–dry cycles in southern Patagonia: chronology, sedimentology and geochemistry of a lacustrine record from Laguna Potrok Aike, Argentina. The Holocene 17, 297–310.

Haberzettl, T., Anselmetti, F.S., Bowen, S.W., Fey, M., Mayr, C., Zolitschka, B., Ariztegui, D., Mauz, B., Ohlendorf, C., Kastner, S., Lücke, A., Schäbitz, F., Wille, M., 2009. Late Pleistocene dust deposition in the Patagonian steppe — extending and refining the paleoenvironmental and tephrochronological record from Laguna Potrok Aike back to 55 ka. Quat. Sci. Rev. 28, 2927–2939.

Halley, R.B., 1977. Ooid fabric and fracture in the Great Salt Lake and the geologic record. J. Sed. Petrol. 47, 1099–1120.

Heegaard, E., Birks, H.J.B., Telford, R.J., 2005. Relationships between calibrated ages and depth in stratigraphical sequences: an estimation procedure by mixed-effect regression. The Holocene 15, 612–618.

Holmes, J., 2001. Ostracoda. In: Smol, J.P., Last, W.M., Birks, H.J. (Eds.), Tracking environmental change using lake sediments. Zoological indicators, 4. Kluwer Academic Publishers, Dordrecht, The Netherland, pp. 125–152.

Hua, Q., Barbetti, M., 2004. Review of tropospheric bomb ^{14}C data for carbon cycle modeling and age calibration purposes. Radiocarbon 46, 1273–1298.

ImageJ, 2013. http://rsbweb.nih.gov/ij/.

Irurzún, M.A., Gogorza, C.S.G., Chaparro, M.A.E., Lirio, J.M., Nuñez, H., Vilas, J.F., Sinito, A.M., 2006. Paleosecular variations recorded by Holocene–Pleistocene sediments from Lake El Trébol (Patagonia, Argentina). Phys. Earth Planet. Inter. 154, 1–17.

Jansen, J.H.F., van der Gaast, S.J., Koster, B., Vaars, A.J., 1998. CORTEX, a shipboard XRF-scanner for element analyses in split sediment cores. Mar. Geol. 151, 143–153.

Kasten, S., Zabel, M., Heuer, V., Hensen, C., 2003. Processes and signals of nonsteady-state diagenesis in deep-sea sediments and their pore waters. In: Wefer, G., Mulitza, S., Rathmeyer, V. (Eds.), Sonderforschungsbereich 261. Springer-Verlag, Berlin, pp. 431–459.

Kelts, K., Briegel, U., Ghilardi, K., Hsü, K., 1986. The limnogeology-ETH coring system. Schweiz. Z. Hydrol. 48, 104–115.

Kilian, R., Lamy, F., 2012. A review of glacial and Holocene paleoclimate records from southernmost Patagonia (49–55°S). Quat. Sci. Rev. 53, 1–23.

Kirschvink, J.L., 1980. The least-squares line and plane and the analysis of palaeomagnetic data. Geophys. J. R. Astron. Soc. 62, 699–718.

Kylander, M.E., Ampel, L., Wohlfarth, B., Veres, D., 2011. High-resolution X-ray fluorescence core scanning analysis of Les Echets (France) sedimentary sequence: new insights from chemical proxies. J. Quat. Sci. 26, 109–117.

Lamy, F., Kilian, R., Arz, H.W., Francois, J.-P., Kaiser, J., Prange, M., Steinke, T., 2010. Holocene changes in the position and intensity of the southern westerly wind belt. Nat. Geosci. 3, 695–699.

Larsen, D., 1994. Origin and paleoenvironmental significance of calcite pseudomorphs after ikaite in the Oligocene Creede Formation, Colorado. J. Sediment. Res. 64, 593–603.

Lisé-Pronovost, A., St-Onge, G., Gogorza, C., Haberzettl, T., Preda, M., Kliem, P., Francus, P., Zolitschka, B., 2013. High-resolution paleomagnetic secular variations and relative paleointensity since the Late Pleistocene in southern South America. Quat. Sci. Rev. 71, 91–108.

Mancini, M.V., Franco, N.V., Brook, G.A., 2013. Palaeoenvironment and early human occupation of southernmost South America (South Patagonia, Argentina). Quat. Int. 299, 13–22.

Marchant, R., Hooghiemstra, H., 2004. Rapid environmental change in African and South American tropics around 4000 years before present: a review. Earth Sci. Rev. 66, 217–260.

Markgraf, V., Bradbury, J.P., Schwalb, A., Burns, S.J., Stern, C., Ariztegui, D., Gilli, A., Anselmetti, F.S., Stine, S., Maidana, N., 2003. Holocene palaeoclimates of southern Patagonia: limnological and environmental history of Lago Cardiel, Argentina. The Holocene 13, 581–591.

Martens, K., Behen, F., 1994. A Checklist of the Non-marine Ostracods (Crustacea, Ostracoda) from South-American Inland Waters and Adjacent Islands.

Massaferro, J., Brooks, S.J., 2002. Response of chironomids to Late Quaternary environmental change in the Taitao Peninsula, southern Chile. J. Quat. Sci. 17, 101–111.

Massaferro, J.I., Moreno, P.I., Denton, G.H., Vandergoes, M., Dieffenbacher-Krall, A., 2009. Chironomid and pollen evidence for climate fluctuations during the Last Glacial Termination in NW Patagonia. Quat. Sci. Rev. 28, 517–525.

Massaferro, J., Recasens, C., Larocque-Tobler, I., Zolitschka, B., Maidana, N.I., 2013a. Major lake level fluctuations and climate changes for the past 16,000 years as reflected by diatoms and chironomids preserved in the sediment of Laguna Potrok Aike, southern Patagonia. Quat. Sci. Rev. 71, 167–174.

Massaferro, J.I., Ortega, R., Fuentes, C., Araneda, A., 2013b. Clave para la identificación de Tanytarsini (INSECTA: Diptera: Chironomidae: Chironominae) cuaternarios de la Patagonia. Ameghiniana 50, 319–334.

Mayr, C., Wille, M., Haberzettl, T., Fey, M., Janssen, S., Lücke, A., Ohlendorf, C., Oliva, G., Schäbitz, F., Schleser, G.H., Zolitschka, B., 2007. Holocene variability of the southern hemisphere westerlies in Argentinean Patagonia (52°S). Quat. Sci. Rev. 26, 579–584.

Mayr, C., Lücke, A., Maidana, N.I., Wille, M., Haberzettl, T., Corbella, H., Ohlendorf, C., Schäbitz, F., Fey, M., Janssen, S., Zolitschka, B., 2009. Isotopic fingerprints on lacustrine organic matter from Laguna Potrok Aike (southern Patagonia, Argentina) reflect environmental changes during the last 16,000 years. J. Paleolimnol. 42, 81–102.

Mayr, C., Lücke, A., Wagner, S., Wissel, H., Ohlendorf, C., Haberzettl, T., Oehlerich, M., Schäbitz, F., Wille, M., Zhu, J., Zolitschka, B., 2013. Intensified southern hemisphere westerlies regulated atmospheric CO_2 during the last deglaciation. Geology 41, 831–834.

Mazaud, A., 2005. User-friendly software for vector analysis of the magnetization of long sediment cores. Geochem. Geophys. Geosyst. 6.

McCormac, F., Hogg, A., Blackwell, P., Buck, C., Higham, T., Reimer, P., 2004. SHCal104 southern hemisphere calibration 0–11.0 cal kyr BP. Radiocarbon 46, 1087–1092.

Mees, F., Castaneda, C., Herrero, J., Van Ranst, E., 2011. Bloedite sedimentation in a seasonally dry saline lake (Salada Mediana, Spain). Sediment. Geol. 238, 106–115.

Meisch, C., 2000. Freshwater Ostracoda of Western and Central Europe. In: Schwoerbel, J., Zwick, P. (Eds.), Suesswasserfauna von Mitteleuropa 8/3. Spektrum Akademischer Verlag, Heidelberg, Berlin, p. 522pp.

Moreno, P.I., Francois, J.P., Villa-Martinez, R.P., Moy, C.M., 2009. Millennial-scale variability in southern hemisphere westerly wind activity over the last 5000 years in SW Patagonia. Quat. Sci. Rev. 28, 25–38.

Moreno, P.I., Francois, J.P., Moy, C.M., Villa-MartÃnez, R., 2010. Covariability of the Southern Westerlies and atmospheric CO_2 during the Holocene. Geology 38, 727–730.

Movia, C.P., Soriano, A., León, R.J.C., 1987. La vegetación de la Cuenca del Río Santa Cruz (Provincia de Santa Cruz, Argentina). Darwiniana 28, 9–78.

Müller, P.J., Schneider, R., 1993. An automated leaching method for the determination of opal in sediments and particulate matter. Deep-Sea Res. 40, 425–444.
NCDC, 2011. NNDC Climate Data Online. National Climatic Data Center.
Oehlerich, M., Mayr, C., Griesshaber, E., Lücke, A., Oeckler, O.M., Ohlendorf, C., Schmahl, W.W., Zolitschka, B., 2013. Ikaite precipitation in a lacustrine environment — implications for palaeoclimatic studies using carbonates from Laguna Potrok Aike (Patagonia, Argentina). Quat. Sci. Rev. 71, 46–53.
Ohlendorf, C., Sturm, M., 2001. Precipitation and dissolution of calcite in a Swiss High Alpine Lake. Arct. Antarct. Alp. Res. 33, 410–417.
Ohlendorf, C., Gebhardt, A.C., Hahn, A., Kliem, P., Zolitschka, B., the PASADO science team, 2011. The PASADO core processing strategy — a proposed new protocol for sediment core treatment in multidisciplinary lake drilling projects. Sediment. Geol. 239, 104–115.
Ohlendorf, C., Fey, M., Gebhardt, C., Haberzettl, T., Lücke, A., Mayr, C., Schäbitz, F., Wille, M., Zolitschka, B., 2013. Mechanisms of lake-level change at Laguna Potrok Aike (Argentina) — insights from hydrological balance calculations. Quat. Sci. Rev. 71, 27–45.
Oliva, G., González, L., Rial, P., Livraghi, E., 2001. El ambiente en la Patagonia Austral. In: Borrelli, P., Oliva, G. (Eds.), Ganadería ovina sustentable en la Patagonia Austral - tecnología de manejo extensivo. INTA Centro Regional Patagonia Sur, Río Gallegos, Santa Cruz, Argentina, pp. 19–82.
Paruelo, J.M., Beltrán, A., Jobbágy, E., Sala, O.E., Golluscio, R.A., 1998. The climate of Patagonia: general patterns and controls on biotic processes. Ecol. Aust. 8, 85–101.
Ramón Mercau, J., Laprida, C., Massaferro, J., Rogora, M., Tartari, G., Maidana, N., 2012. Patagonian ostracods as indicators of climate-related hydrological variables: implications for paleoenvironmental reconstructions in Southern South America. Hydrobiologia 694, 235–251.
Recasens, C., Ariztegui, D., Gebhardt, C., Gogorza, C., Haberzettl, T., Hahn, A., Kliem, P., Lisé-Pronovost, A., Lcke, A., Maidana, N., Mayr, C., Ohlendorf, C., Schäbitz, F., St-Onge, G., Wille, M., Zolitschka, B., Team, P.S., 2011. New insights into paleoenvironmental changes in Laguna Potrok Aike, southern Patagonia, since the Late Pleistocene: the PASADO multiproxy record. The Holocene 22, 1323–1335.
Reimer, P.J., Brown, T.A., Reimer, R.W., 2004. Discussion: reporting and calibration of post-bomb ^{14}C data. Radiocarbon 46, 1299–1304.
Roberts, N., Eastwood, W.J., Kuzucuoglu, C., Fiorentino, G., Caracuta, V., 2011. Climatic, vegetation and cultural change in the eastern Mediterranean during the mid-Holocene environmental transition. The Holocene 21, 147–162.
Roland, T.P., Caseldine, C.J., Charman, D.J., Turney, C.S.M., Amesbury, M.J., 2014. Was there a '4.2 ka event' in Great Britain and Ireland? Evidence from the peatland record. Quat. Sci. Rev. 83, 11–27.
Rosetti, G., Martens, K., 1998. Taxonomic revision of the recent and Holocene representatives of the family Darwinulidae (Crustacea, Ostracoda), with a description of three new genera. Bull. K. Belg. Inst. Nat. Wet. 68, 55–110.
Rothwell, R.G., Hoogakker, B., Thomson, J., Croudace, I.W., Frenz, M., 2006. Turbidite emplacement on the southern Balearic Abyssal Plain (western Mediterranean Sea) during Marine Isotope Stages 1–3: an application of ITRAX XRF scanning of sediment cores to lithostratigraphic analysis. In: Rothwell, R.G. (Ed.), New Techniques in Sediment Core Analysis. Geological Society of London, Special Publications, London, pp. 79–98.
Schäbitz, F., Wille, M., Francois, J.-P., Haberzettl, T., Quintana, F., Mayr, C., Lücke, A., Ohlendorf, C., Mancini, V., Paez, M.M., Prieto, A.R., Zolitschka, B., 2013. Reconstruction of palaeoprecipitation based on pollen transfer functions — the record of the last 16 ka from Laguna Potrok Aike, southern Patagonia. Quat. Sci. Rev. 71, 175–190.
Schimpf, D., Kilian, R., Kronz, A., Simon, K., Spötl, C., Wörner, G., Deininger, M., Mangini, A., 2011. The significance of chemical, isotopic, and detrital components in three coeval stalagmites from the superhumid southernmost Andes (53°S) as high-resolution palaeo-climate proxies. Quat. Sci. Rev. 30, 443–459.
Schwalb, A., Burns, S.J., Cusminsky, G., Kelts, K., Markgraf, V., 2002. Assemblage diversity and isotopic signals of modern ostracodes and host waters from Patagonia, Argentina. Palaeogeogr. Palaeoclimatol. Palaeoecol. 187, 323–339.
Stoner, J.S., St-Onge, G., 2007. Chapter three magnetic stratigraphy in paleoceanography: reversals, excursions, paleointensity, and secular variation. In: Hillaire-Marcel, C., Anne De, V. (Eds.), Proxies in Late Cenozoic Paleoceanography. Elsevier, pp. 99–137.
Stuiver, M., Reimer, P., 1993. Extended 14C database and revised CALIB radiocarbon calibration program. Radiocarbon 35, 215–230.
Stuiver, M., Reimer, P., Reimer, R., 2005. Calib 5.0 [WWW program and documentation].
Swainson, I.P., Hammond, R.P., 2001. Ikaite, $CaCO_3{\bullet}6H_2O$: cold comfort for glendonites as paleothermometers. Am. Mineral. 86, 1530–1533.
Teller, J.T., Bowler, J.M., Macumber, P.G., 1982. Modern sedimentation and hydrology in Lake Tyrrell, Victoria. J. Geol. Soc. Aust. 29, 159–175.
Thomson, J., Croudace, I.W., Rothwell, R.G., 2006. A geochemical application of the ITRAX scanner to a sediment core containing eastern Mediterranean sapropel units. In: Rothwell, R.G. (Ed.), New Techniques in Sediment Core Analysis. Geological Society of London Special Publications, London, pp. 65–77.
Ülgen, U.B., Franz, S.O., Biltekin, D., Cagatay, M.N., Roeser, P.A., Doner, L., Thein, J., 2012. Climatic and environmental evolution of Lake Iznik (NW Turkey) over the last ~4700 years. Quat. Int. 274, 88–101.
van Geel, B., Heusser, C.J., Renssen, H., Schuurmans, C.J.E., 2000. Climatic change in Chile at around 2700 BP and global evidence for solar forcing: a hypothesis. The Holocene 10, 659–664.
Varma, V., Prange, M., Merkel, U., Kleinen, T., Lohmann, G., Pfeiffer, M., Renssen, H., Wagner, A., Wagner, S., Schulz, M., 2012. Holocene evolution of the southern hemisphere westerly winds in transient simulations with global climate models. Clim. Past 8, 391–402.
Verbruggen, F., Heiri, O., Meriläinen, J.J., Lotter, A.F., 2011. Subfossil chironomid assemblages in deep, stratified European lakes: relationships with temperature, trophic state and oxygen. Freshw. Biol. 56, 407–423.
Vollenweider, R.A., Kerekes, J., 1982. Eutrophication of waters. Monitoring, assessment and control. OECD Cooperative Programme on Monitoring of Inland Waters (Eutrophication Control). OECD, Paris.
Waldmann, N., Ariztegui, D., Anselmetti, F.S., Austin, J.A., Moy, C.M., Stern, C., Recasens, C., Dunbar, R.B., 2010. Holocene climatic fluctuations and positioning of the southern hemisphere westerlies in Tierra del Fuego (54° S), Patagonia. J. Quat. Sci. 25, 1063–1075.
Walker, I., 1990. Modern assemblages of arctic and alpine Chironomidae as analogues for late-glacial communities. Hydrobiologia 214, 223–227.
Wilkinson, B.H., Pope, B.N., Owen, R.M., 1980. Nearshore ooid formation in a modern temperate region marl lake. J. Geol. 88, 697–704.
Zamora, L., Mezquita, F., Julia, R., Armengol, X., Riera, S., Currás, A., Reed, J.M., Marqués, M.A., Alonso, N., 2009. Palaeoecological reconstruction of Lake Estany d'Ivars-Vila-Sana (Northeastern Spain) based on ostracod remains and other proxies. XVI International Symposium on Ostracoda. July 26–30, Brasilia (Brazil Abstracts, 064 pp.).
Zolitschka, B., Corbella, H., Maidana, N., Ohlendorf, C., 2006a. Investigating maar formation and the climate history of southern Argentina — the Potrok Aike Maar Lake Sediment Archive Drilling Project (PASADO). Sci. Drill. 3, 54–55.
Zolitschka, B., Schäbitz, F., Lücke, A., Corbella, H., Ercolano, B., Fey, M., Haberzettl, T., Janssen, S., Maidana, N., Mayr, C., Ohlendorf, C., Oliva, G., Paez, M.M., Schleser, G., Soto, J., Tiberi, P., Wille, M., 2006b. Crater lakes of the Pali Aike Volcanic Field as key sites for paleoclimatic and paleoecological reconstructions in southern Patagonia, Argentina. J. S. Am. Earth Sci. 21, 294–309.
Zolitschka, B., Anselmetti, F., Ariztegui, D., Corbella, H., Francus, P., Lücke, A., Maidana, N.I., Ohlendorf, C., Schäbitz, F., Wastegård, S., 2013. Environment and climate of the last 51,000 years — new insights from the Potrok Aike maar lake Sediment Archive Drilling prOject (PASADO). Quat. Sci. Rev. 71, 1–12.